

The Infrared Ca II triplet as metallicity indicator

R. Carrera and C. Gallart

Instituto de Astrofísica de Canarias, Spain

rcarrera@iac.es

carme@iac.es

E. Pancino

Osservatorio Astronomico di Bologna, Italy

and

R. Zinn

Department of Astronomy, Yale University, USA

ABSTRACT

From observations of almost 500 RGB stars in 29 Galactic open and globular clusters, we have investigated the behaviour of the infrared Ca II triplet (8498, 8542 and 8662 Å) in the age range $13 \leq \text{Age}/\text{Gyr} \leq 0.25$ and the metallicity range $-2.2 \leq [\text{Fe}/\text{H}] \leq +0.47$. These are the widest ranges of ages and metallicities in which the behaviour of the Ca II triplet lines has been investigated in a homogeneous way. We report the first empirical study of the variation of the CaII triplet lines strength, for given metallicities, with respect to luminosity. We find that the sequence defined by each cluster in the Luminosity- ΣCa plane is not exactly linear. However, when only stars in a small magnitude interval are observed, the sequences can be considered as linear. We have studied the the Ca II triplet lines on three metallicities scales. While a linear correlation between the reduced equivalent width (W'_V or W'_I) versus metallicity is found in the Carretta & Gratton (1997) and Kraft & Ivans (2003) scales, a second order term needs to be added when the Zinn & West (1984) scale is adopted. We investigate the role of age from the wide range of ages covered by our sample. We find that age has a weak influence on the final relationship. Finally, the relationship derived here is used to estimate the metallicities of three poorly studied open clusters: Berkeley 39, Trumpler 5 and Collinder 110. For the latter, the metallicity derived here is the first spectroscopic estimate available.

Subject headings: stars: abundances — stars: late-type — globular clusters: general — open clusters: individual (Berkeley 39, Collinder 110, Trumpler 5)

1. Introduction

The main functions defining the star formation history of a complex stellar system are the star formation rate, $\text{SFR}(t)$ and the chemical enrichment law, $Z(t)$, both function of time. The $\text{SFR}(t)$ can be derived in detail from deep color–magnitude diagrams. $Z(t)$ has been traditionally constrained by the color distribution of RGB stars. However, this method of deriving metallicities from photometry is a very crude one because in the RGB there is a degeneracy between age and metallicity. To break this degeneracy we may obtain metallicities from another source and then derive the age from the positions of stars in the color–magnitude diagram. Of course, the best way to obtain stellar metallicities is high-resolution spectroscopy, which also provides abundances of key chemical elements. However, a lot of telescope time is necessary to measure a suitable number of stars. The alternative is low-resolution spectroscopy, which allows us to observe a large number of stars in a reasonable time using modern multi-object spectrographs. At low resolution, the metallicity is obtained from a spectroscopic line strength index. The Mg_2 , Ca II H & K and Ca II infrared triplet lines, the Fe lines, etc., are the most widely used indexes for obtaining stellar metallicities. Different indexes are adequate for different types of stars. For example, Fe lines are useful for stars at the base of the RGB or in the main sequence turn-off. Observation of these stars, however, is only possible for the closest systems and even those require 8 m-class telescopes and long integration times. Thus, for external galaxies, the only stars that can be observed with modern multi-object spectrographs and reasonable amounts of telescope time are those near the tip of the RGB. A good spectroscopic index to obtain metallicities for these stars is the infrared Ca II triplet (CaT), whose lines are the strongest features in the infrared spectra of red giant stars.

Armandroff & Zinn (1988) demonstrated that in the integrated spectra of Galactic globular clusters, the equivalent widths of CaT lines are strongly correlated with metallicity. As the near-infrared light of globular clusters, where the CaT lines are, is dominated by the red giant contribution, this relation may be also true in these stars individually. Subsequent studies focused on the analysis of individual red giants in globular clusters (e.g. Armandroff & Da Costa 1991). These studies demonstrated that the strength of the CaT lines changes systematically with luminosity along the RGB. Moreover, for a given luminosity, the strength of these lines is correlated with the cluster metallicity. Many authors have obtained empirical relationships between the combined equivalent width of the CaT

lines and cluster metallicity. A very comprehensive work in this field was published by Rutledge et al. (1997a), based on 52 Galactic globular clusters covering a metallicity range of $-2 \leq [\text{Fe}/\text{H}] \leq -0.7$. They compared the resulting calibration in the Zinn & West (1984) and Carretta & Gratton (1997) metallicity scales. While in the Carretta & Gratton (1997) scale a linear correlation between metallicity and equivalent width of the CaT lines at the level of the horizontal-branch (HB) $V-V_{HB}=0$ (known as reduced equivalent width) was found for all clusters, this relationship was not linear when the Zinn & West (1984) scale was used. In most studies, the run of CaT lines with metallicity has been investigated in globular clusters only, which have all similar ages. If we wish to derive stellar metallicities in systems in which star formation has taken place in the last few Gyr, such as dwarf irregular galaxies or open clusters, it is necessary to address the role of age on the CaT strength. Some authors have used (a few) young open clusters to study the behaviour of the CaT with metallicity (e.g. Suntzeff et al. 1992), using the Zinn & West (1984) metallicity scale as reference. Cole et al. (2004) very recently obtained a new relationship, using open and globular clusters covering $-2 \leq [\text{Fe}/\text{H}] \leq -0.2$ and $2.5 \leq (\text{age}/\text{Gyr}) \leq 13$ in the Carretta & Gratton (1997) scale. They found a linear correlation among the reduced equivalent width and metallicity. This indicates a weak influence of age in the range of ages investigated (age ≥ 2.5 Gyr). However, to apply this relationship to systems with star formation over the last Gyr and/or with stars more metal-rich than the solar metallicity, it is necessary to investigate its behaviour further for younger ages and higher metallicities.

The purpose of this paper is to obtain a new relationship between the equivalent width of the CaT lines and metallicity, covering a range as wide as possible of age and metallicity. Our sample covers $-2.2 \leq [\text{Fe}/\text{H}] \leq +0.47$ and $0.25 \leq \text{Age}/\text{Gyr} \leq 13$. The influence of age and the variation of the CaT lines along the RGB are investigated. In Section 2, we present the cluster sample. In Section 3, the observations and data reduction are described. The way in which the equivalent width of the the CaT lines has been computed is described in Section 4, where the behaviour of the CaT with luminosity is also investigated. In Section 5 we obtain the relationship between the equivalent width of the CaT lines and metallicity, and we discuss the influence of age and the $[\text{Ca}/\text{Fe}]$ ratio in them. Finally, the derived relationships are used in Section 6 to obtain the metallicities of the open clusters Berkeley 39, Trumpler 5 and Collinder 110.

2. Clusters Sample

To study the behaviour of the CaT lines with metallicity, we have observed individual stars, with available V magnitudes, in 29 stellar clusters (15 open and 14 globular). Of

the 29 clusters in this sample, 27 also have I magnitudes available. This sample covers the widest range of ages ($0.25 \leq \text{Age/Gyr} \leq 13$) and metallicities ($2.2 \leq [\text{Fe}/\text{H}] \leq +0.47$) in which the CaT lines have been observed in a homogeneous way. The main parameters of the observed clusters are listed in Table 1. Our sample covers most of the open clusters visible from the northern hemisphere with enough stars above the red clump to get a good sampling of the RGB, and with magnitudes easily reachable with the INT, WHT and 2.2 m CAHA telescopes. In particular, the sample contains NGC 6705 (M11), a very young open cluster (0.25 Gyr) with a well populated RGB, and NGC 6791, one of the oldest open clusters (~ 9 Gyr), which is among the most metal-rich clusters in our Galaxy ($[\text{Fe}/\text{H}] \sim +0.47$). From the south, using the VLT¹ and CTIO 4 m telescope, we observed four globular clusters, including NGC 5927 and NGC 6528, which are among the most metal-rich globular clusters in our Galaxy. The sample also includes the observations of 9 globular and 3 open clusters available at the ESO archive, whose observations were carried out with the same instrumental configurations as our own. With the purpose of investigating the behaviour of the CaT lines with luminosity, we have observed stars along the RGB in 5 clusters spanning our whole range of metallicities.

Table 1 presents a list of all the clusters in our sample, together with their main characteristics: age, distance modulus, reddening, reference metallicities in 3 scales (see Section) and $[\text{Ca}/\text{H}]$. In total, 26 of the 29 observed clusters have metallicities in at least one of the three scales. For the other 3 clusters (Collinder 110, Trumpler 5 and Berkeley 39), we calculate their metallicities with the relationships obtained here.

3. Observations and Data Reduction

About 500 stars have been observed in the 29 clusters of our sample in 6 different runs from 2002 to 2005, using the William Herschel Telescope (WHT) and Isaac Newton Telescope (INT), both at Roque de los Muchachos Observatory (La Palma, Spain), the 4 m telescope at CTIO (La Serena, Chile), the 2.2 m at the Calar Alto Observatory (Almeria, Spain) and the VLT at Paranal Observatory (Chile). The dates, instruments and spectral resolution for each run are listed in Table 2. The instrumental configurations have been chosen in order to ensure that the resolution was similar in each run. The exposure times were selected as a function of the magnitude of the stars in order to obtain a good S/N, which in most cases was greater than 20. We have rejected from the analysis those stars with S/N lower than

¹Based on observations made with ESO telescopes at Paranal observatories under programme 074.B-0446(B).

20 (see below). In each run we have observed a few stars in common with other runs in order to ensure the homogeneity of our sample. Equivalent widths obtained for each star observed in two or more runs have been plotted in Figure 1. The differences between runs are $< 0.1 \pm 0.1 \text{ \AA}$. The calculated equivalent widths, together with the obtained radial velocity and the utilized V and I magnitudes, are listed in Table 3.

The data taken with slit spectrographs, i.e., all except the observations with HYDRA@CTIO and WYFFOS@WHT, were reduced following the procedure described by Massey et al. (1992) using the IRAF² packages but with some small differences described by Pont et al. (2004). We obtained two images of each object, with the star shifted along the slit. First, we subtracted the bias and overscan, and corrected by the flat-field. Then, since the star is in a different physical position in the two images, we subtracted one from the other, obtaining a positive and a negative spectrum in the same image. With this procedure the sky is subtracted in the same physical pixel in which the star was observed, thus minimizing the effects of pixel to pixel sensitivity variations. Of course, a time dependency remains since the two spectra have not been taken simultaneously. These sky residues are eliminated in the following step, when the spectrum is extracted in the traditional way and the remaining sky background is subtracted from the information on both sides of the star aperture. As the next step, the spectrum is wavelength calibrated. We then again subtracted the negative from the positive (so we added both spectra because one is negative) to obtain the final spectrum. Finally, each spectrum was normalized by fitting a polynomial, excluding the strongest lines in the wavelength range such as those of the CaT. The order of the polynomial changes among runs in order to eliminate the response of each instrument. The wavelength calibration of the VLT data (both from the archive and from run 6) might be less accurate than the rest because arcs are not taken at the same time and with the same telescope pointing as the object. The effects of this on the wavelength calibration has discussed by Gallart et al. (2001), and we evaluate them in Section ???. However, since we are not interested in obtaining precise radial velocities, this problem will not have an important impact on our project.

HYDRA@CTIO and WYFFOS@WHT are multifibre spectrographs. The data obtained with HYDRA has been extracted with the DOHYDRA task within IRAF in the way described by Valdes (1992). This task was developed specially to extract data acquired with this instrument. The procedure is described in depth by Carrera et al. (2007). Basically, after bias, overscan subtraction and trimming, DOHYDRA traces the apertures, makes the

²IRAF is distributed by the National Optical Astronomy Observatory, which is operated by the Association of Universities for Research in Astronomy, Inc., under cooperative agreement with the National Science Foundation.

flat-field correction and calibrates in wavelength. We followed a similar procedure with the data obtained with WYFFOS, but in this case we used the general DOFIBERS task, which works similarly to DOHYDRA. Although both tasks allow for sky subtraction, the results were poor, and important residuals of sky lines remained. To remove the contribution of these sky lines, we have developed our own procedure to subtract them. Basically, it consists in obtaining an average sky spectrum from all fibres placed on the sky in a given configuration. Before subtracting this average, high S/N sky, from each star spectrum, we need to know the relation between the intensity of the sky in each fibre (which varies from fibre to fibre due to the different fibre responses) and the average sky. This relation is a weight (which may depend on wavelength) by which we must multiply the average sky spectra before subtracting it from each star. To calculate it, we have developed a task that finds the weight which minimizes the sky line residuals over the whole spectral region considered. As a result of this procedure, the sky emission lines are removed very accurately. Finally, the normalization was carried out in the same way as previously described.

Examples of 4 stars with different metallicities are shown in Figure 2. Note how the strength of the CaT lines increases with metallicity.

The radial velocity of each star has been calculated in order to reject cluster non-members. We used the FXCOR task in IRAF, which performs the cross-correlation between the target and template spectra of known radial velocity (Tonry & Davis 1979). We selected between 8 and 10 template stars in each run that had very high S/N and covered a wide range of radial velocities. The velocities were corrected to the heliocentric reference frame within FXCOR. The final radial velocity for each star was obtained as the average of the velocities obtained from each template, weighted by the width of correlation peaks.

In the case of observations with slit spectrographers, the star might not be exactly positioned in the centre of the slit. This error means a velocity uncertainty given by $\Delta v = c \times \Delta\Theta \times p/\lambda_0$, where: c is the light speed, p is the spectral resolution given in \AA arcsec^{-1} ; λ_0 is the wavelength of the lines (in this case $\sim 8600 \text{ \AA}$), and $\Delta\Theta$ is the angular offset of the star from the centre of the slit in arcsec. This effect has been described by Irwin & Tolstoy (2002) and Harris & Zaritsky (2006). In our case, it may only be significant in the case of the VLT observations. To estimate the offset in this case we used through-slit images obtained at the beginning of the observation of each configuration, taken to check that the stars were positioned in the slits. In this image we have measured the position of each stellar centroid, which is compared with the position of the slit given in the header of the image. The difference between both, $\Delta\Theta$, allows us to calculate the uncertainty in the measurement of the radial velocity. This value changes from one star to another, the error being about 15 km s^{-1} on average.

The mean velocity for each cluster is listed in Table 4. Most of the values obtained agree, within the uncertainties, with previous measurements from the literature, even in the case of the clusters observed with the VLT, where the uncertainties are larger. In the case of NGC 2141, we found a mean velocity similar to the value obtained by Cole et al. (2004). Both values differ by 20 and 30 km s⁻¹, respectively, from the value found by Friel et al. (2002). For Collinder 110, no previous measurement of its radial velocity could be found in the literature.

4. The Calcium Triplet

We are interested in obtaining metallicities from red giant stars, and within this group, from the brightest ones, which are of spectral types K and M. The main features in the infrared spectra of these stars are the CaT lines. But their spectra also contains other weak atomic lines. The Fe I (8514.1, 8674.8, 8688.6 and 8824.2 Å) and Ti I (8435.0 Å) lines are the most important. When within this range, we move to later spectral types, and hence to cooler stars, molecular bands begin to appear that change the slope of the local continuum. The main contribution are from the titanium oxide (TiO) bands, the strongest of which are the triplet situated at 8432, 8442 and 8452 Å and the doublet at 8859.6 and 8868.5 Å. There are other weaker bands at 8472, 8506, 8513, 8558 and 8569 Å, near the bluest lines of the CaT. There are also several vanadium oxide (VO) bands at 8521, 8538, 8574, 8597, 8605, 8624, 8649 and 8668 Å. The strength of these features increases when the temperature decreases, i.e. when we move to later spectral types. The presence of these bands complicates the definition of the continuum, which makes it difficult to obtain the equivalent widths of the CaT lines for stars with $T_{eff} \leq 3500$ K or $(V-I) > 2$, in the most metal-rich clusters. The description of the CaT region for other spectral types can be found in Cenarro et al. (2001).

4.1. Definition of Line and Continuum Bandpass Windows

In the literature we can find different prescriptions to measure the strength of the CaT lines. The classical definition of a spectral index consists in establishing a central bandpass covering a spectral feature and one or more bandpasses on both sides to trace the local continuum reference level. Cenarro et al. (2001) have presented a description of the previous CaT index definitions and a comparison among them. In Figure 3 we have plotted the line and continuum bandpasses used in several reference works, Cenarro et al. (2001) (a), Rutledge et al. (1997a) (b) and Armandroff & Zinn (1988) (c), over a metal-poor (left) and a metal-rich (right) spectrum. The Armandroff & Zinn (1988) and Rutledge et al. (1997a)

indices were defined for relatively metal-poor RGB stars where the influence of the molecular bands is not important. The index of Cenarro et al. (2001) was defined specifically to avoid the presence of molecular bands. Also, from Figure 3, we can easily see that the wings of the lines are larger than the line bandpasses defined by Armandroff & Zinn (1988) and Rutledge et al. (1997a) in the case of the metal rich stars. Only the line bandpasses defined by Cenarro et al. (2001) completely cover the line wings. Although we have selected the bandpasses defined by Cenarro et al. (2001), which are listed in Table 5, the equivalent width of the line will be measured in a different way, as described in the following section.

4.2. Equivalent widths

The next step is to measure the line flux from its equivalent width. The equivalent width of a spectral line can be measured in different ways. One method is by numerical integration of the observed spectra in a line band (e.g. Cenarro et al. 2001). However, in the wings of the strongest lines of the CaT there are some weak lines, whose strength may change with different stellar atmospheric parameters than the CaT lines. These lines must be excluded when we measure the CaT equivalent width. The alternative (e.g. Rutledge et al. 1997a; Cole et al. 2004) consists in fitting an empirical function to a line profile and calculating the equivalent width from the integration of this fit. Many functions have been used to fit the CaT line profiles, most commonly a Gaussian profile (e.g. Armandroff & Da Costa 1991). However, as Cole et al. (2004) have shown, the Gaussian profile provides a good fit for weak-line stars, but the fit is worse in strong-line stars, where the contribution of the non-Gaussian wings of the CaT lines becomes substantial. We have to take this point into account because the main contributors to the strength of the CaT lines are their wings, while the core is not very sensitive to the atmosphere and stellar parameters (Erdelyi-Mendes & Barbuy 1991). Rutledge et al. (1997a) fitted a Moffat function of exponent 2.5. As Pont et al. (2004) has demonstrated, the behaviour of Moffat function of exponent 2.5 is similar to the Gaussian fit for the weakest lines. However, neither provides a good fit to the strongest lines. Cole et al. (2004) fitted the whole line profile with the sum of a Gaussian and a Lorentzian function, which provides a better fit for the strongest lines and agrees with the single Gaussian fit for the weakest lines (see Cole et al. 2004, for a further discussion). We have compared the different functions in order to evaluate the quality of the fit in the whole range of line strengths. We have chosen the sum of a Gaussian and a Lorentzian function because this provides the best fit for the whole range of equivalent widths in this study. We have also checked whether a simple Gaussian or Moffat function would produce a good fit in the case of spectra obtained with lower resolution. Also in this case a Gaussian plus a Lorentzian provides the best fit for strong-line stars.

A Gaussian plus a Lorentzian function has therefore been fitted to the line profiles with a least-squares method, using the Levenberg-Marquardt algorithm. For the whole range of equivalent widths covered in this work, the differences between the observed line and the fit are negligible for stars with $S/N \geq 20$. Stars with poorer S/N have been rejected. The equivalent width of each line is the area limited by the fitted profile of the line and the continuum level, defined as the linear fit to the mean values of the flux in each window chosen to determine the continuum. Formal errors of the fit are estimated as the difference between the equivalent width measurement for continuum displacements of $\pm(S/N)^{-1}$.

4.3. The CaT index

The equivalent widths of the three CaT lines are combined to form the global index ΣCa (Armandroff & Da Costa 1991). Some authors excluded the weakest line at 8498 Å on the basis of its poor S/N (e.g. Suntzeff et al. 1993; Cole et al. 2000). Others have used all three lines, either weighted (e.g. Rutledge et al. 1997a) or unweighted (e.g. Olszewski et al. 1991). As our spectra have high S/N ratios, we used the unweighted sum of the three lines, $\Sigma Ca = W_{8498} + W_{8542} + W_{8662}$, and we calculate its error as the square root of the quadratic sum of the errors of each line. As we have some stars in common with previous works, we can compare the ΣCa calculated by us with values obtained in previous papers. Rutledge et al. (1997a) compared their ΣCa with previous index definitions until 1997. Here, for simplicity, we are only going to compare our index with three reference works. Stars in common with Armandroff & Da Costa (1991); Rutledge et al. (1997a) and Cole et al. (2004) are plotted in Figure 4. As mentioned before, the works of Armandroff & Da Costa (1991) and Rutledge et al. (1997a) were focused on old and metal-poor stars. However, Olszewski et al. (1991) and Suntzeff et al. (1993), using the same index as Armandroff & Da Costa (1991) defined for globular cluster stars, measured the equivalent width of the CaT lines in stars of two open clusters, M11 and M67, respectively. We are going to use these values to complete the measurements of Armandroff & Da Costa (1991).

We find a quasilinear relation up to $\Sigma Ca \sim 7$ among the ΣCa values in this paper and those obtained by Armandroff & Da Costa (1991) (see also Suntzeff et al. 1993). From this point the relationship saturates: while our index increases by an additional $\Delta \Sigma Ca \sim 2$, theirs only increases by $\Delta \Sigma Ca \sim 1.5$ (on their scale). We believe that the reason for this is that they fitted the line profile by a Gaussian function which underestimates the contribution of the line wings in strong lines (see Section). Note also the zero-point difference between both scales. The relation is not exactly one to one because they did not use the equivalent width of the weakest CaT line. However, the slope close to one of the linear fit for the

metal-poor stars implies that the two indices are almost equivalent for these kind of stars. The loss of linearity for strong-line stars partly explains why these authors found a nonlinear relationship between the CaT index and metallicity, but, of course, the metallicity scale also plays a role in this issue, as we discuss in Section 5.2. The linear fit for $\Sigma\text{Ca}_{\leq 7}$ (solid straight line in top panel of Figure 4) is:

$$\Sigma Ca_{AC91} = -0.88(\pm 0.08) + 0.96(\pm 0.01)\Sigma Ca_{TP} \quad (1)$$

and the second order polynomial fit for the whole range of equivalent widths is

$$\Sigma Ca_{AC91} = -1.10(\pm 0.08) + 1.20(\pm 0.03)\Sigma Ca_{TP} - 0.04(\pm 0.01)\Sigma Ca_{TP}^2 \quad (2)$$

In the case of Rutledge et al. (1997a), who only observed stars with $[\text{Fe}/\text{H}] \leq -0.7$, we find a linear correlation for the whole range of equivalent widths. In this case the slope is less than one, meaning that their index is less sensitive to changes in the strength of the CaT lines than ours. For the same star, our index is higher than the Rutledge et al. (1997a) one. The linear fit is:

$$\Sigma Ca_{R97} = -0.23(\pm 0.06) + 0.78(\pm 0.01)\Sigma Ca_{TP}. \quad (3)$$

Finally, the correlation between Cole et al. (2004) index and ours is one to one ($\Sigma Ca_{TP} - \Sigma Ca_{C04} = 0.009 \pm 0.0007$). As we used the same empirical function and index definition of ΣCa as Cole et al. (2004), differences could only come from the definition of line and continuum bandpasses. This means that, in the range of equivalent widths covered here, both indices are equivalent. However, as the continuum in our index has been defined to avoid the influence of TiO bands, we expect that our index would also behave well in stars whose continuum is contaminated by TiO bands.

4.4. The reduced equivalent width

The next step is to relate the CaT index with metallicity. The strength of the absorption lines mainly depends on the chemical abundance, stellar effective temperature (T_{eff}) and surface gravity ($\log g$). Therefore, to relate the equivalent width of the CaT lines with

metallicity it is necessary to remove the T_{eff} and $\log g$ dependence. Armandroff & Da Costa (1991) and Olszewski et al. (1991) demonstrated that the cluster stars define a sequence in the Luminosity– ΣCa plane, using luminosity measures from indicators like M_I or $(V - V_{HB})$. These sequences are separated as a function of the cluster metallicity. The theoretical explanation of this can be found in Pont et al. (2004), using Jørgensen et al. (1992) models, which describe the behaviour of the CaT lines as a function of T_{eff} , $\log g$ and metallicity.

It is necessary to study the morphology of the sequence defined by each cluster in the Luminosity– ΣCa plane. From a theoretical point of view, the increment of luminosity along the RGB comes with a drop in T_{eff} and $\log g$ that decreases and increases the strength of the lines, respectively. The result is a modest increment in ΣCa with luminosity ($\delta \Sigma Ca / \delta M_I \sim 0.5$). Moreover, the models predict that ΣCa increases more rapidly with luminosity in the upper part of the RGB (above the HB) than in the lower part. In other words, the sequence defined by each cluster might not be linear and might be best described adding a quadratic component. The Jørgensen et al. (1992) models also predict that ΣCa increases more rapidly when $\log g$ decreases, or when the luminosity increases, for the more metal-rich clusters than for the more metal-poor ones. Therefore, the linear and quadratic terms, which characterize the sequence defined for each cluster in the luminosity– ΣCa plane, increase with metallicity, as can be seen in Figure 15 of Pont et al. (2004).

Observationally, the variation in ΣCa with metallicity has traditionally been studied from $(V - V_{HB})$, which removes any dependence on distance and reddening (e.g. Armandroff & Da Costa 1991; Rutledge et al. 1997a; Cole et al. 2004). In this context, it is found that clusters define linear sequences in the $(V - V_{HB})$ – ΣCa plane, where the reduced equivalent width, W' , is defined as $\Sigma Ca = W'_{HB} + \beta(V - V_{HB})$. Rutledge et al. (1997a) found that the slopes of these sequences were the same for all clusters in their sample, independently of their metallicity. Therefore only W'_{HB} changes from one cluster to another, and its variation is directly related to metallicity. Other studies have reached the same conclusion using open and globular clusters (e.g. Olszewski et al. 1991). Pont et al. (2004) (see also Armandroff & Da Costa 1991) have demonstrated that this also occurs in the M_V – ΣCa and M_I – ΣCa planes. However, no studies have observed the theoretical predictions that cluster sequences are not exactly linear with luminosity, or that their shape depends on metallicity.

The main objective of this study is to apply the relationships obtained to derive metallicities of individual stars in Local Group galaxies, which in general have had multiple star formation epochs and do not always have a well defined HB (e.g. LMC: Carrera et al. 2007; SMC: Noël et al. 2007; Leo A: Cole et al. 2007). For example, the Magellanic Clouds do not have a measurable HB in the CMD, and in studies which define the reduced equivalent width as a function of $(V - V_{HB})$ (e.g. Cole et al. 2005), the HB position has been taken

as that of the red-clump. However, in the Magellanic Clouds, the position of the red-clump is about 0.4 magnitudes brighter than the HB. This only implies underestimating the metallicity by $\simeq 0.15$ dex, which is similar to the uncertainty on the metallicity determination itself. Distances to Local Group galaxies are in general determined with an accuracy greater than 0.4 mag., and so, even if the error on the derived metallicity due to the uncertainty in the position of the HB is not large, it can be minimized by defining the reduced equivalent width as a function of absolute magnitude. This point is also important in the case of open clusters, which hardly ever have a HB or, if they do, it is usually not well defined. For this reason, like Pont et al. (2004), we redefine W' as the value of ΣCa at $M_V=0$ (hereafter W'_V) or $M_I=0$ (hereafter W'_I).

First we will study in detail the morphology of the cluster sequences in the Luminosity– ΣCa plane. As discussed above, from a theoretical point of view, we expect that these sequences are not exactly linear. We have observed stars along the RGB in 5 clusters covering the whole metallicity range. In Figure 5 we have plotted stars observed in these clusters in the M_V – ΣCa and M_I – ΣCa planes. These stars have magnitudes in the ranges $-2 \leq M_V \leq 2$ and $-3 \leq M_I \leq 2$ (or $-2.3 \leq V - V_{HB} \leq 1.8$). These ranges contain both stars brighter and fainter than previous works (e.g. Rutledge et al. 1997a; Cole et al. 2004). Note that the strength of the CaT lines increases more rapidly in the upper part of the RGB, as predicted by Pont et al. (2004) using Jørgensen et al. (1992) models. These observations can be used to obtain a new relationship between ΣCa , absolute magnitude and metallicity valid for all the stars in the RGB, that takes into account the curvature in the Luminosity– ΣCa plane. The sequence of each cluster has been fitted with a quadratic function such that $\Sigma Ca = W'_{V,RGB} + \beta M_V + \gamma M_V^2$. We plotted the result when the stars of each cluster are fitted independently in Figure 5. The coefficients of the fit are shown in Table 6. From this, it seems that β tends to increase with metallicity, as predicted theoretically. In the case of γ this increment is not observed, i.e. its variation does not show a significant dependence on metallicity, except for the most metal-rich cluster, which also has a large uncertainty.

Using the Jørgensen et al. (1992) empirical relations and the BaSTI stellar evolution models (Pietrinferni et al. 2004), we have calculated theoretical sequences for clusters with $[Fe/H] \geq -1$, which are plotted in Figure 6 as dashed lines. These models were obtained for $[Fe/H] = +0.5, 0, -0.5$ and -1 , while the clusters metallicities are $[Fe/H] = +0.47, -0.14, -0.67$ and -1.07 respectively. Jørgensen et al. (1992) did not compute relationships for more metal-poor clusters. We used BaSTI isochrones with metallicities of $+0.32, -0.28, -0.58$ and -0.98 , respectively, in order to estimate T_{eff} and $\log g$ along the RGB. The Jørgensen et al. (1992) relationships were calculated for the two strongest CaT lines. To compare the theoretical predictions with the observational sequences we computed, using our own data, an empirical relation between $\Sigma Ca_{8442+8662}$ obtained from these two lines

and the ΣCa used in this work, computed from the three CaT lines. We found is $\Sigma Ca = 0.13 + 1.21\Sigma Ca_{8442+8662}$. Applying this correction, we find that the theoretical and observed cluster sequences still do not match. There is a zero-point that changes from one cluster to another, which is not surprising because the cluster metallicities are not exactly the same as those used to compute the theoretical relationships. Therefore, the theoretical sequences have been shifted in order to superimpose them on the cluster ones. It can be seen that models do not exactly reproduce the behaviour of the observed cluster sequences. However, the prediction that the shape changes from the metal-poor clusters to the metal-rich ones is observed, although, as was mentioned before, these variations are similar to the uncertainties.

We can simplify the problem if we assume that all clusters have the same tendency, i.e. if we calculate a single slope and quadratic term for the whole sample. So only the zero point changes among clusters. To obtain these coefficients, we have performed an iterative least-squares fit as described by Rutledge et al. (1997a). From a set of reference values, we obtained the quadratic and linear terms of the fit in iterative steps, until they converged to a single value within the errors and allow only the zero point to change among clusters. The values are: $\beta_V = -0.647 \pm 0.005$ and $\gamma_V = 0.085 \pm 0.006$. In the same way, for M_I we obtained $\beta_I = -0.618 \pm 0.005$ and $\gamma_I = 0.046 \pm 0.001$. In Figure 6 we have plotted the individual fit for each cluster (solid line) and that when the linear and quadratic terms do not change among clusters (dashed lines). In both cases, the dotted lines represent the region where there are no cluster stars and the fits have therefore been extrapolated. As we can see in Figure 6, in the magnitude interval covered by cluster stars, both fits are similar and give very similar values of W' within the uncertainties. For example, for NGC 7078, where the discrepancy is larger, we obtained 2.79 ± 0.06 and 2.79 ± 0.01 in V ; and 2.64 ± 0.08 and 2.31 ± 0.01 in I , when the linear and quadratic terms change among clusters or they are fixed, respectively. Larger differences between both fits are found in the regions where the relationships are extrapolated.

Moreover, in our case we are interested in measuring the strength of the CaT lines in galaxies where we can observe only the upper part of the RGB with a good S/N. The quadratic behaviour of the cluster sequences in the Luminosity– ΣCa plane is not significant when we observe stars with $M_I \leq 0$ only (or $M_V \leq 1.25$; this magnitude limit has been selected in order to sample in both filters the same number of stars in each cluster). For example, when we repeat the previous procedure, but only for stars with $M_V \leq 1.25$, we find that the quadratic term is $\gamma_V = 0.004 \pm 0.003$, which is negligible within the uncertainty. In the same way, when we only observe stars with $M_V \geq 1.25$ we obtain a similar result: $\gamma_V = 0.002 \pm 0.01$. The same happens in the M_I – ΣCa plane, but here the quadratic terms are even smaller. According to this, the cluster sequence can be considered linear above and below $M_V = 1.25$ and $M_I = 0$, and we can fit it as $\Sigma Ca = W'_V + \beta_V M_V$ or $\Sigma Ca = W'_I + \beta_I M_I$ on each side of this

point. Following the same iterative procedure as in the case of the quadratic fit, we calculated the values of the slope β for $M_V \leq 1.25$ and for $M_I \leq 0$, obtaining $\beta_V = -0.74 \pm 0.01$ and $\beta_I = -0.60 \pm 0.01$, respectively. The linear fits for $M_V \leq 1.25$ and $M_I \leq 0$ are represented in Figure 6, by dotted–dashed lines. In all cases, within the ranges covered by the cluster stars, the linear fit to the bright stars is equivalent, within the uncertainties, to the quadratic ones.

Finally, for clusters where we have observed a wide range of magnitudes we find that the slope (β) increases, although within the uncertainties, with metallicity. We might check this point using now all clusters in our sample. A total of 27 clusters in I and 29 in V have stars brighter than $M_I=0$ and $M_V = 1.25$. We have fitted the sequence to each cluster independently in the linear form $\Sigma Ca = W'_{V,I} + \beta_{V,I} M_{V,I}$. The values obtained from the slope have been plotted against W' , which is directly correlated with metallicity, for each cluster in Figure 7. From this figure it is seen that there is no significant relation between the cluster slope and W' (or $[\text{Fe}/\text{H}]$). Therefore, from here on, we consider the slope of the fit to be the same for the whole range of $[\text{Fe}/\text{H}]$ and, hence, for all objects.

In summary, as we are specially interested in obtaining metallicities for stars in the upper part of the RGB with the CaT, where the quadratic term is not significant and the slope can be fixed independently of metallicity, we are going to use a linear fit with a single slope for the calibration using the whole cluster sample. This is what has been done in all previous calibrations of the CaT.

Figures 8 and 9 represent the clusters in our sample in the $M_V-\Sigma Ca$ and $M_I-\Sigma Ca$ planes respectively, together with the linear fit to each of them. Using the same procedure as in the case of the quadratic fit discussed above, we have obtained $\beta_V = -0.677 \pm 0.004$ and $\beta_I = -0.611 \pm 0.002 \text{ \AA mag}^{-1}$ in the $M_V-\Sigma Ca$ and $M_I-\Sigma Ca$ planes, respectively. The value found in the $M_I-\Sigma Ca$ plane is slightly larger than that obtained by Pont et al. (2004), $\beta_I = -0.48 \pm 0.02 \text{ \AA mag}^{-1}$. Although these authors used a different method to calculate the metallicity (they fitted each cluster individually and obtained the mean of the slopes of all of them), this is not the reason for the discrepancy because if we follow the same procedure with our own data, again we find $\beta_I = -0.61$. There are no previous determinations of β_V . The values obtained for W'_V and W'_I are listed in Table 7.

5. The Ca II Triplet metallicity scale

An important point in this study is the reference metallicities. It would be ideal to use the same metallicity scale for both open and globular clusters, and that this would have been obtained from high-resolution spectroscopy. In the literature we can find two globular

cluster metallicity scales obtained from high resolution spectroscopy: Carretta & Gratton (1997, hereafter CG97) and Kraft & Ivans (2003, hereafter KI03). There is a third metallicity scale obtained from low-resolution data: Zinn & West (1984, hereafter ZW84). There are systematic differences among these three scales, but there is no reason to prefer any particular one of them. For this reason, here we are going to study the behaviour of the CaT lines with metallicity in these three scales. Lamentably, there is not a homogeneous metallicity scale obtained from high-resolution spectroscopy for open clusters. However, the metallicities of some of them have been obtained directly in the CG97 scale by some authors: NGC 6819 (Bragaglia et al. 2001); NGC 2506 (Carretta et al. 2004); NGC 6791 (Gratton et al. 2006) and Berkeley 32 (Sestito et al. 2006). These metallicities were obtained using Fe I and Fe II lines. For the other 8 open clusters in our sample there are also metallicities obtained from high-resolution spectroscopy in RGB stars and using Fe I and Fe II lines in a similar way to CG97. Even though some discrepancies could exist because the procedures are not exactly the same, we are considering these metallicities also to be on the CG97 scale. The reference values in this scale are listed in column 2 of Table 1 and the sources for each of them are listed in column 3. The reference metallicities in the ZW84 and KI03 are listed in columns 4 and 5 respectively. In both cases, we have used only values obtained directly by these authors.

5.1. Calibration in the CG97 metallicity scale

Figures 10 and 11 show the run of W'_V and W'_I with metallicity. In most cases, the errors are smaller than the size of the points. The circles indicate clusters younger than 4 Gyr. The solid line shows the best fit to the data. The dashed lines represent the 90% confidence level. Note that in both cases there is a linear correlation. The bottom panels show the residuals of the linear fit. We have used 22 clusters for the calibration in V and 20 for that in I . There are three clusters that differ from the fit by more than 0.2 dex in both filters. These clusters are NGC 2420, NGC 2506 and Berkeley 32. They have been excluded from the analysis. In the case of NGC 2420, only 6 stars in V and 4 in I are radial velocity members. This, together with a relatively large uncertainty in its metallicity (Gratton 2000), contributes to its large error bar. In the case of NGC 2506 and Berkeley 32, there are only 3 and 4 stars respectively with membership confirmed by their radial velocities. Thus, slight differences in the ΣCa value of one of them could change the derived W' significantly. Two of the three very deviant clusters (NGC 2420 and NGC 2506) have ages less than 4 Gyrs, but 5 other young clusters fit the mean relationships in Figures 10 and 11 to better than 0.2 dex. We doubt therefore that cluster age is the major cause of the large deviations.

The best linear fits shown in Figures 10 and 11, are:

$$[Fe/H]_{CG97}^V = -3.12(\pm 0.06) + 0.36(\pm 0.01)W'_V \quad \sigma_V = 0.08 \quad (4)$$

$$[Fe/H]_{CG97}^I = -2.95(\pm 0.06) + 0.38(\pm 0.01)W'_I \quad \sigma_I = 0.09 \quad (5)$$

Some studies have predicted that this relationship may present a curvature due to the loss of CaT index sensitivity at high metallicities (e.g. Díaz et al. 1989). Cole et al. (2004) investigated this point adding a quadratic term. They found that the coefficient of this term is insignificant and does not improve the quality of the fit. We performed the same analysis in our sample, which covers a wider range of ages and metallicities, finding a similarly insignificant influence of a quadratic term.

5.2. Calibration on Other Metallicity Scales

In this section we study the behaviour of the CaT on the ZW84 and KI03 scales. In Figure 12 we have plotted the metallicities in ZW84 (bottom) and KI03 (top) listed in Table 1 versus W'_V (left) and W'_I (right), respectively.

In the case of the KI03 metallicity scale (top panels), the behaviour of W' with metallicity is linear, as for the CG97 scale. These authors used three stellar atmosphere models to obtain metallicities. For simplicity, in Figure 12 we have plotted only the metallicity values obtained using MARCS models. However, a linear behaviour is also found when we use the metallicities computed from the Kurucz models with or without convective overshooting. The linear fits for each of the three models are:

$$[Fe/H]_{KI03}^V = -3.42(\pm 0.03) + 0.37(\pm 0.01)W'_V \quad \sigma = 0.10 \quad (MARCS) \quad (6a)$$

$$[Fe/H]_{KI03}^V = -3.43(\pm 0.03) + 0.38(\pm 0.01)W'_V \quad \sigma = 0.10 \quad (Kurucz \text{ with convective overshooting}) \quad (6b)$$

$$[Fe/H]_{KI03}^V = -3.51(\pm 0.03) + 0.40(\pm 0.01)W'_V \quad \sigma = 0.10 \quad (Kurucz \text{ without convective overshooting}) \quad (6c)$$

$$[Fe/H]_{KI03}^I = -3.29(\pm 0.03) + 0.40(\pm 0.01)W'_I \quad \sigma = 0.09 \quad (MARCS) \quad (7a)$$

$$[Fe/H]_{KI03}^I = -3.24(\pm 0.03) + 0.40(\pm 0.01)W'_I \quad \sigma = 0.09 \quad (Kurucz \text{ with convective overshooting}) \quad (7b)$$

$$[Fe/H]_{KI03}^I = -3.31(\pm 0.03) + 0.41(\pm 0.01)W'_I \quad \sigma = 0.09 \quad (Kurucz \text{ without convective overshooting}) \quad (7c)$$

Differences between metallicities derived with the MARCS model and the models of Kurucz with or without overshooting are negligible.

This linear behaviour is not surprising because, as KI03 demonstrated, their metallicities are linearly correlated with the CG97 values, which are, at the same time, linearly correlated with our W' . However, the metallicities calculated by KI03 are systematically lower than the CG97 ones. KI03 studied this point and concluded that the difference could be explained because they used different T_{eff} and $\log g$ values, as well as different atmosphere models. The combination of all these can easily introduce systematic differences in the globular cluster abundance scales.

In the case of ZW84, we have found that the data are best fitted by a second-degree polynomial (solid line):

$$[Fe/H]_{ZW84}^V = -1.98(\pm 0.07) - 0.18(\pm 0.02)W'_V + 0.05(\pm 0.01)W'^2_V \quad \sigma_V = 0.10 \quad (8a)$$

$$[Fe/H]_{ZW84}^I = -2.07(\pm 0.07) - 0.12(\pm 0.03)W'_I + 0.05(\pm 0.01)W'^2_I \quad \sigma_I = 0.09 \quad (8b)$$

In Section 4.3, we discussed several previous definitions and measurement procedures of the CaT lines, and noted the loss of sensitivity to the CaT lines strength in some cases (e.g. Armandroff and Da Costa 1991) which also found a non-linear relationship between the CaT index and metallicity. We mentioned that this non-linearity was probably the result of the combination of a non-accurate measurement of the CaT on strong-line stars and the particular metallicity scale in use. In order to assess the relative importance each factor, we will now compare the effects on the derived abundances of alternatively i) assuming a linear relationship between W' and metallicity on the ZW84 metallicity scale and ii) adopting a Gaussian to fit the CaT lines, which provides a poorer fit. When a linear relationship between W'_I and $[Fe/H]_{ZW84}$ is assumed, the derived metallicity of a strong-line star, $W'_I=8.5$, is underestimated in 0.3 dex. In the case of a weak-line star, $W'_I=2$, again the metallicity is underestimated in 0.2 dex. Similar results are obtained when lines are not properly fitted. For example, as we saw in Section 4.3, Armandroff & Da Costa (1991) fitted the line profile with a Gaussian, resulting in that their index saturated for strong-line stars. The relation between the reduced equivalent width obtained from their index and metallicities in the CG97 scale is a second-degree polynomial. If we then assume a linear relationship between this index and $[Fe/H]_{CG97}$ for a strong-line star, its metallicity would be underestimated in 0.3 dex. Similar result is obtained for a weak-line star. We conclude therefore, that the effects on the derived metallicity due to a poor fit to the line or the non-linearity of the metallicity scale are comparable.

5.3. The role of Age in the W'_V (W'_I) versus [Fe/H] relationship

Pont et al. (2004) investigated the influence of age in the W'_V (W'_I) versus [Fe/H] relationship from a theoretical point of view. They used the theoretical calculations of CaT equivalent widths for different values of $\log g$, T_{eff} and metallicity calculated by Jørgensen et al. (1992) together with the Padova stellar evolution models (Girardi et al. 2002). They concluded that the variation of W' with age for a fixed metallicity would be negligible for clusters older than 4 Gyr. However, this was not the case for the younger clusters. This is observed clearly in Figure 15 by Pont et al. (2004). For a given metallicity, the sequences in the M_V - ΣCa and M_I - ΣCa planes are separated as a function of their ages for clusters younger than ~ 4 Gyr. According to this calculation, for the same metallicity, W' decreases with age. Thus, metallicities for clusters younger than 4 Gyr, calculated from calibrations computed from old stars, will be underestimated. This age dependence is more important in the M_V - ΣCa plane than in the M_I - ΣCa one. This means that W'_I would be less sensitive to age than W'_V .

Using the Jørgensen et al. (1992) models and the BaSTI stellar evolution models (Pietrinferni et al. 2004), we have estimated the expected W' differences as a function of age. From these calculations, for two clusters with the same metallicity and age 10.5 and 0.6 Gyr respectively, the youngest cluster W'_V would be approximately 0.7 Å lower than that of the oldest one. This implies that the metallicity obtained for young clusters using this calibration would be 0.25 dex more metal-poor than the actual metallicity. In the case of W'_I , the difference would be 0.4 Å, so the metallicity obtained for young clusters would be 0.15 dex more metal-poor than the actual one. As we can see in Figure 15 by Pont et al. (2004), the difference would be similar for different metallicities.

From our data, we confirm that the influence of age is weak. In Figure 13 we plot W'_I versus age for clusters with $-0.17 \leq [\text{Fe}/\text{H}]_{CG97} \leq +0.07$. We have selected this range because it contains clusters with a wide range of ages and is small enough for the metallicity differences to be within the uncertainties. We can see that clusters with ages younger than 5 Gyr (NGC 2141, NGC 2682, NGC 6819 and NGC 7789) have similar W'_I than the oldest one (NGC 6528). There are only two clusters that deviate widely from the behaviour of the others. One of these is the youngest cluster, NGC 6705, which has a larger W'_I than the oldest clusters. This is contrary to the theoretical prediction that it should be smaller. However, we have to take into account that differences of 0.5 Å in W'_I mean differences of ~ 0.1 dex in [Fe/H]. So the observed variations are similar to the uncertainty in the determination of [Fe/H]. Our data are not accurate enough to detect the influence of age because the uncertainty in the metallicity determination of clusters is similar to the expected variations due to age.

5.4. The influence of [Ca/Fe] abundance

The CaT has traditionally been used to infer Iron abundances from Ca lines, and we also do so in this paper. But, the CaT lines strength should also be sensitive to the Ca abundances. In fact, the relationships obtained in this work and those found in the literature have been obtained assuming implicitly the specific relationship between Ca and Fe followed by clusters used in the calibration (see Figure 14 for the relationship of the clusters used in this work). Using these relationships to derive Fe abundances in stellar systems with a different chemical evolution than the Milky Way, reflected in the calibrating cluster sample, could give wrong results.

In general, the relationship between the reduced equivalent width of an atomic line and the chemical abundance of the corresponding element is described by the curve of growth. This is only linear for very weak and unsaturated lines. This is not the case for the CaT. As we can find the [Ca/H] ratio for most of the clusters in our sample from the literature, in Figure 14 we have plotted W'_V and W'_I versus [Ca/H]. The relationship between both is equivalent to the curve of growth. The relations obtained are:

$$[Ca/H]^V = -2.51(\pm 0.08) + 0.30(\pm 0.01)W'_V \quad \sigma = 0.11 \quad (9)$$

$$[Ca/H]^I = -2.36(\pm 0.08) + 0.31(\pm 0.01)W'_I \quad \sigma = 0.11 \quad (10)$$

As in the case of the [Fe/H] relationship, we obtain a linear dependence. However, note that in this case the errors of the fit are larger. This may be related to the inhomogeneity of the [Ca/H] abundances, which were obtained from different sources.

In any case, even though [Ca/H] changes linearly with W' , [Fe/H] does not have to do likewise. However, as we see in Figures 10 and 11, the relationship between [Fe/H] and W' is also linear. On the other hand, since the [Ca/H] and [Ca/Fe] abundances are related according to $[Fe/H] = [Ca/H] - [Ca/Fe]$, we can expect that [Ca/Fe] also changes linearly with W' (and with [Fe/H]), if the relation with [Ca/H] is linear. In fact, in Figure 14 we can check that this is the case over the whole range of [Fe/H] except for the most metal-poor clusters. Note however that the linear behaviour of W' with [Ca/H] and [Ca/Fe] is a characteristic of our particular sample, but this would not have to be the rule.

The problem of the relation between the CaT, [Ca/H] and [Fe/H] has been addressed by Idiart et al. (1997) from an empirical point of view. For their sample of late-type stars (G and K), they found that the dominant stellar parameter controlling the behaviour of the CaT lines is metallicity, and contrary to what would be expected, the [Ca/Fe] ratio has practically no effect on the CaT index. However, all the stars in their sample follow the

same relationship between Ca and Fe, so they cannot check in a general way the influence of the [Ca/Fe] ratio.

To properly investigate the influence of the [Ca/Fe] ratio, it is necessary to have objects with the same metallicities and different [Ca/H] ratios. In our sample, most of the metal-poor clusters have high α -element abundances relative to Fe, as is the case for Ca. On the other hand, open clusters are metal-rich and have low α -element abundances. To study the influence of the [Ca/Fe] ratio on the CaT calibration as a function of metallicity it would be necessary to include metal-rich objects with high α -element abundances (i.e. stars in the Milky Way bulge) and metal-poor objects with low α -element abundances (i.e. perhaps stars in dwarf galaxies). This sort of work would need a huge observational effort, which explains why it has not been done until now.

6. Derived cluster Metallicities

We will use the relationships derived in previous sections to estimate the metallicities in the three observed clusters without previous determinations. In fact, we have observed Collinder 110, a poorly studied cluster with no previous spectroscopic metallicity determinations. For Berkeley 39, only Friel et al. (2002) have determined its metallicity from low-resolution spectroscopy. The sequences of these clusters in the M_I - ΣCa plane have been plotted in Figure 16.

6.1. Berkeley 39

The first colour–magnitude diagram of this open cluster was published by Kaluzny & Richtler (1989). These authors calculated a distance modulus of $(m-M)_V = 13.4$ and $E(B-V) = 0.12$. These values agree with the determinations of Carraro et al. (1994), who also used colour–magnitude diagrams. The age of this cluster is 7 ± 1 Gyr (Salaris et al. 2004).

There are few determinations of its metallicity. From photometric data Twarog et al. (1997) estimated $[Fe/H] = -0.18 \pm 0.03$, while from low-resolution spectroscopy, Friel & Janes (1993) and Friel et al. (2002) obtained $[Fe/H] = -0.32 \pm 0.08$ and $[Fe/H] = -0.26 \pm 0.09$ respectively. In our case we have 10 RGB stars which are cluster members from their radial velocity, although only 5 stars have I magnitudes available. Moreover, only 2 are brighter than $M_I = 0$; nevertheless, the other 3 have magnitudes close to this value. We therefore used all 5 stars. From Equation 5 we obtain $[Fe/H]_{CG97} = -0.14 \pm 0.02$. We have used the relationship as a function of M_I because the RGB is more resolved in the I filter, and

this relation is less sensitive to age. The calculated value is slightly more metal-rich than previous spectroscopic determinations. In the KI03 and ZW84 scales we obtain $[\text{Fe}/\text{H}]_{\text{KI03}} = -0.33 \pm 0.14$ and $[\text{Fe}/\text{H}]_{\text{ZW84}} = -0.23 \pm 0.25$ respectively from Equations 7a and 8b. On these scales we have no young and/or metal-rich reference clusters, but, as we have checked before, the influence of age is weak.

We have also calculated the radial velocity of this cluster. We find $V_r = 59 \pm 5 \text{ km s}^{-1}$, which is similar to values found previously (i.e. Friel et al. 2002, $V_r=55\pm 7 \text{ Km s}^{-1}$).

6.2. Trumpler 5

Trumpler 5, also named Collinder 105, is also a poorly studied cluster, even though it was discovered about 75 yr ago. It is located towards the Galactic anticentre in a rich star field in Monoceros, and in a region of variable interstellar reddening. This has complicated the studies of this cluster. In fact, only photometric studies could be found in the literature (e.g. Kaluzny 1998; Kim & Sung 2003; Piatti et al. 2004) with the exception of the work by Cole et al. (2004), who observed the CaT lines in a few stars on the RGB and derived the first spectroscopic determination of its metallicity. The distance modulus and reddening of this cluster have been derived from isochrone fitting. Most studies converge on a reddening of $E(B - V) = 0.6$ (e.g. Kim & Sung 2003). However, this does not happen in the case of the distance, where the values lie between $(m-M)_0 = 12.25$ (Piatti et al. 2004) and 12.64 (Kim & Sung 2003), corresponding to a distance from the Sun of 2.4 or 3.4 kpc respectively. Also, the age and metallicity have traditionally been estimated from isochrones. The age of this cluster is estimated between 2.4 ± 0.2 (Kim & Sung 2003) and 5.0 ± 05 Gyr (Piatti et al. 2004), while the derived metallicity is $[\text{Fe}/\text{H}] = -0.30 \pm 0.15$ dex (e.g. Kim & Sung 2003; Piatti et al. 2004).

We have observed 21 stars in the field of Trumpler 5, 17 of which are radial velocity members (Table 3). The metallicity derived from Equation 5 is $[\text{Fe}/\text{H}]_{\text{CG97}} = -0.36 \pm 0.05$, which is more metal-rich (although within the error) than the previous spectroscopic determination, $[\text{Fe}/\text{H}] = -0.56 \pm 0.11$, by Cole et al. (2004). The alternative determination of the metallicity on the KI03 and ZW84 scales gives $[\text{Fe}/\text{H}]_{\text{KI03}} = -0.56 \pm 0.09$ and $[\text{Fe}/\text{H}]_{\text{ZW84}} = -0.48 \pm 0.20$ respectively from Equations 7a and 8b

From our data we have also calculated the radial velocity of this cluster, $V_r = 44 \pm 10 \text{ km s}^{-1}$, which is similar to the value derived by Cole et al. (2004, $V_r=54\pm 5 \text{ Km s}^{-1}$).

6.3. Collinder 110

Collinder 110 is a poorly populated cluster, even less studied than Trumpler 5. Only two photometric studies can be found in the literature for the last three decades. Using synthetic colour–magnitude diagrams, Bragaglia & Tosi (2003) have estimated a reddening of $0.38 \leq E(B - V) \leq 0.45$ and distance modulus $(m-M)_0$ between 11.8 and 11.9. From these values they derived an age between 1.1 and 1.5 Gyr. Similar values were found by Dawson & Ianna (1998). There are no metallicity determinations for this cluster in the literature. Bragaglia & Tosi (2003) tried to derive the metallicity of this cluster from different stellar evolution models, but concluded that the final result vary widely depending on the models.

The metallicity derived from Equation 5 is $[\text{Fe}/\text{H}]_{CG97} = -0.01 \pm 0.07$. If we use Equations 7a and 8b on KI03 and ZW84 metallicity scales we find $[\text{Fe}/\text{H}]_{KI03} = -0.19 \pm 0.21$ and $[\text{Fe}/\text{H}]_{ZW84} = 0.00 \pm 0.30$. From our data we can also provide the first determination of its radial velocity, $V_r = 45 \pm 8 \text{ km sec}^{-1}$.

7. Summary

We have observed the CaT lines in RGB stars in a sample of 29 clusters of the Milky Way. This sample covers an age range of ($13 \leq \text{Age}/\text{Gyr} \leq 0.25$) and metallicity range of ($-2.2 \leq [\text{Fe}/\text{H}] \leq +0.47$). These are the widest ranges of ages and metallicities in which the behaviour of the CaT has been investigated in a homogeneous way until now. We have obtained relationships between the CaT equivalent widths and metallicities on the scales of Zinn & West (1984), Carretta & Gratton (1997) and Kraft & Ivans (2003). The influence of other parameters, such as age and $[\text{Ca}/\text{Fe}]$ ratio, has been investigated. Moreover, for the first time, the behaviour of the CaT lines as a function of luminosity along the RGB has been studied for the whole range of metallicities in our sample.

The main results of this work are:

- Theoretically, it has been predicted that the sequences of clusters in the Luminosity– ΣCa plane may not be linear, and that the slope should change with metallicity. In this article we have demonstrated that the nonlinear tendency and the change of the slope can be (marginally) detected if a wide range of magnitudes in the RGB is observed.
- However, this behaviour is not significant if only the usual range of 3-4 magnitudes below the tip of the RGB is observed. For this reason, for stars with $M_V \leq 1.25$ or

$M_I \leq 0$, we have considered that the sequences of the clusters in the $M_V-\Sigma Ca$ and $M_I-\Sigma Ca$ planes are linear, and share a common slope, independently of metallicity.

- We have obtained relationships between the reduced equivalent width (W'_V and W'_I) and metallicity on the Zinn & West (1984), Carretta & Gratton (1997) and Kraft & Ivans (2003) scales. While on the Carretta & Gratton (1997) and Kraft & Ivans (2003) scales these relationships are linear, in the case of the Zinn & West (1984) scale, it is quadratic.
- Theory predicts that the relationship between the CaT line equivalent widths and metallicity might be dependent on age, mainly for clusters younger than 4 Gyr. We have studied the influence of age and found that the expected differences due to age are similar to the metallicity resolution of our work.
- We have also investigated the influence of Ca abundances on the relationships between W'_V and W'_I and metallicity. We have found that $[Ca/H]$ also changes linearly with W'_V and W'_I .
- Finally, the relationships obtained have been used to compute the metallicity of 3 clusters in our sample: Berkeley 39, Trumpler 5 and Collinder 110. For the last one, there are no previous determinations of its metallicity in the literature.

We warmly thank Dr. Antonio Aparicio for many fruitful discussions on this paper, and a careful and critical reading of the manuscript. Extensive use was made of the WEBDA database, maintained at the university of Geneva, Switzerland. C.G. and R.C. acknowledge the support from the Spanish Ministry of Science and Technology (Plan Nacional de Investigación Científica, Desarrollo, e Investigación Tecnológica, AYA2004-06343). E. P. acknowledge support from the Italian MIUR (Ministero dell'Università e della Ricerca) under PRIN 2003029437 entitled "Continuities and discontinuities in the formation of the galaxy". R.Z. acknowledges the support of the NSF under grant AST05-07364.

Facilities: VLT(FORS2), CAHA2.2m(CAFOS), CTIO4m(HYDRA), WHT(WYFFOS), WHT(ISIS), INT(IDS).

REFERENCES

- Alcaino, G., 1974, A&AS, 13, 55
- Alcaino, G., & Liller, W. 1980, AJ, 96, 92

- Alcaino, G., & Liller, W. 1986, A&A, 161, 61
- Armandroff, T. E., & Zinn, R. 1988, AJ, 96, 92
- Armandroff, T. E. & Da Costa, G. S. 1991, AJ, 101, 1329
- Bragaglia, A., Carretta, E., Gratton, R. G., Tosi, M., Bonanno, G., Bruno, P., Calí, A.,
Claudi, R., Cosentino, R., Desidera, S., Farisato, G., Rebeschini, M. & Scuderi, S.
2001, AJ, 121, 327
- Bragaglia, A., & Tosi, M. 2003, MNRAS, 343, 306
- Brown, J. A., Wallerstein, G., & Gonzalez, G. 1999, AJ, 118, 1245
- Buonanno, R., Buscema, G., Corsi, C. E., Iannicola, M. & Fusi Pecci, F. 1983, A&AS, 51,
83
- Burkhead, M. S., Burgess, R. D., & Haisch, B. M. 1972, AJ, 77, 661
- Carraro, G. Chiosi, C., Bressan, A., & Bertelli, G. 1994, A&AS, 103, 375
- Carraro, G. Hassan, S. M., Ortolani, S., & Vallerini, A. 2001, A&A, 372, 879
- Carrera, R., Gallart, C., Hardy, E., Aparicio, A., Zinn, R. 2007, AJ, In preparation
- Carretta, E., & Gratton, R. G. 1997, A&AS, 121, 95 (CG97)
- Carretta, E., Cohen, J. G., Gratton, R. G. & Behr, B. B. 2001, AJ, 122, 1469
- Carretta, E., Bragaglia, A., Gratton, R. G. & Tosi, M. 2004, A&A, 422, 951
- Cenarro, A. J., Cardiel, N., Gorgas, J., Peletier, R. F., Vazdekis, A., & Prada, F. 2001,
MNRAS, 326, 959
- Cole, A. A., Smecker-Hane, T. A., & Gallagher III, J. S. 2000, AJ, 120, 1808
- Cole, A. A., Smecker-Hane, T. A., Tolstoy, E., Bosler, T. L., & Gallagher III, J. S. 2004,
MNRAS, 347, 367
- Cole, A. A., Tolstoy, E., Gallagher III, J. S., & Smecker-Hane, T. A., 2005, AJ, 129, 1465
- Díaz, A. I., Terlevich, E. & Terlevich R. 1989, MNRAS, 239, 325
- Dawson, D. W., & Ianna, P. A. 1998, AJ, 115, 1076
- Erdelyi-Mendes, M., & Barbuy, B. 1991, A&A, 241, 176

- Feltzing, S., & Johnson, R. A. 2002, *A&A*, 385, 67
- Friel, E. D. 1989, *PASP*, 101, 244
- Friel, E. D., & Janes, K. A. 1993, *A&A*, 267, 75
- Friel, E. D., Janes, K. A., Tavares, M., Scott, J., Katsanis, R., Lotz, J., Hong, L., & Miller, N. 2002, *AJ*, 124, 2693
- Fullton, L. K. 1996, *PASP*, 108, 545
- Gallart, C., Martínez-Delgado, D., Gómez-Flechoso, M. A., & Mateo, M. 2001, *AJ*, 121, 2572
- Gim, M., Vanderverg, D. A., Stetson, P. B., Hesser, J. E., & Zurek, D. R. 1998, *PASP*, 110, 1318
- Girardi, L., Bertelli, G., Bressan, A., Chiosi, C., Groenewegen, M: A. T., Marigo, P., Salasnich, B., & Weiss, A. 2002, *A&A*, 391, 195
- Gonzalez, G., & Wallerstein, G. 2000, *PASP*, 112, 1081
- Gratton, R. G. 1987, *A&A*, 179, 181
- Gratton, R. G. 2000, on ASP Conf. Ser. 198, *Stellar Clusters and Associations*, ed. R. Pallavicini, G. Micela & S. Sciortino (San Francisco: ASP), 225
- Gratton, R. G., & Contarini, G. 1994, *A&A*, 283, 911
- Gratton, R. G., Bragaglia, A., Carretta, E., & Tosi, M. 2006, *ApJ*, 642, 462
- Gratton, R. G., & Ortolami, S. 1989, *A&A*, 211,41 *ApJ*, 642, 462
- Harris, J. & Zaritsky, D. 2006, *AJ*, 131, 2514
- Harris, W. E. 1975a, *AJ*, 82, 954
- Harris, W. E. 1975b, *ApJS*, 29, 397
- Harris, W. E. 1982, *ApJS*, 50, 573
- Harris, W. E. 1996, *AJ*, 112, 1487
- Hubbs, L. M., Thorburn, J. A. & Rodriguez-Bell, T. 1990, *AJ*, 100, 710
- Idiart, T. P., Thévenin, F. & de Freitas Pacheco, J. A.. 1997, *AJ*, 113, 1066

- Irwin, M., & Tolstoy, E. 2002, MNRAS, 336, 643
- Jørgensen, U. G., Carlsson, M., & Johnson, H. R. 1992, A&A, 254, 258
- Kaluzny, J., & Richtler, T. 1989, Acta Astron., 39, 139
- Kaluzny, J., 1998, Astron. Astrophys. Suppl. Ser. 133, 25
- Kassis, M., Janes, K. A., Friel, E. D., & Phelps, R. L. 1997, AJ, 113, 1723
- Kim, S. C., & Sung, H., 2003, J. Korean Astron. Soc., 36, 13
- Kraft, R. P., & Ivans, I. I. 2003, PASP, 115, 143 (KI03)
- Layden, A. C., & Sarajedini, A. 1997, ApJ, 486, L110
- Lee, S. W. 1977, A&AS, 27, 381
- Lee, S. K., Kang, Y. W., & Ann, H. B. 1999, PKAS, 14, 61
- Marconi, G., Hamilton, D., Tosi, M., & Bragaglia, A. 1997, MNRAS, 291, 763
- Massey, P., Valdes, F., & Barnes, J. 1992, A User's Guide to Reducing Slit Spectra with IRAF
- Mathieu, R. D. 1985, IAUS, 113, 427
- Mathieu, R. D., Latham, D. W., Griffin, R. F., & Gunn, J. E. 1986, AJ, 92, 1100
- McWilliam, A., Geisler, D., & Rich, R. M. 1992, PASP, 104, 1193
- Mermilliod, J. C. 1995 on "Information and On-line Data in Astronomy", Eds. D. Egret & M. A. Albrecht (Kluwer Academic Press, Dordrecht) p. 127 (<http://obswww.unige.ch/webda>)
- Noël, N., Gallart, C., Costa, E. & Méndez, R.A. 2007, AJ, accepted.
- Olszewski, E. W., Schommer, R. A., Suntzeff, N. B., & Harris, H., C. 1991, AJ, 101, 515
- Origlia, L., Valenti, E., & Rich, R. M. 2005, A&A, 356, 1276
- Ortolani, S., Bica, E., & Barbuy, B. 1992, A&AS, 92, 441
- Piatti, A. E., Calriá, J. J., & Ahumada, A. V. 2004, MNRAS, 349, 641
- Pietrinferni, A., Cassisi, S., Salaris, M., & Castelli, F. 2004, ApJ, 612, 168

- Pont, F., Zinn, F., Gallart, C., Hardy, E., & Winnick, R. 2004, *AJ*, 127, 840
- Richtler, T., & Sagar, R. 2001, *Bull. Astr. Soc. India*, 29, 53
- Rosenberg, A., Saviane, I., Piotto, G., & Aparicio, A. 1999, *AJ*, 118, 2306
- Rosenberg, A., Piotto, G., Saviane, I., & Aparicio, A. 2000, *A&AS*, 144, 5
- Rosenberg, A., Recio-Blanco, A., & García-Marín, M. 2004, *ApJ*, 603, 135
- Rosvick, J. M. 1995, *MNRAS*, 277, 1379
- Rosvick, J. M. & Vandenberg, D. A. 1998, *AJ*, 115, 1516
- Rutledge, G. A., Hesser, J. E., Stetson, P. B., Mateo, M., Simard, L., Bolte, M., Friel, E. D., & Copin, Y. 1997a, *PASP*, 109, 883
- Rutledge, G. A., Hesser, J. E., & Stetson, P. B. 1997b, *PASP*, 109, 907
- Salaris, M., & Weiss, A. 2002, *A&A*, 388, 492
- Salaris, M., Weiss, A., & Percival, S. M. 2004, *A&A*, 414, 163
- Sarajedini, A., von Hippel, T., Kozhurina-Platais, V., & Demarque, P. 1999, *AJ*, 118, 2294
- Sestito, P., Bragaglia, A., Randich, R., Carretta, E., Prisinzano, L. & Tosi, M. 2006, *A&A*, 456, 121
- Shetrone, M. D., & Keane, M. J. 2000, *AJ*, 119, 840
- Snedden, C., Kraft, R. P., Shetrone, M. D., Smith, G. H., Langer, G. E., & Prosser, C. F. 1997, *AJ*, 114, 1964
- Stetson, P. B. 1981, *AJ*, 86, 687
- Stetson, P. B. 2000, *PASP*, 112, 925
- Stetson, P. B., & Harris, W. E. 1977, *AJ*, 82, 954
- Stetson, P. B., Bruntt, H., & Grundahl, F. 2003, *PASP*, 115, 413
- Sung, H., Bessel, M. S., Lee, H. W., Kang, Y. H., Lee, S. W. 1999 *MNRAS*, 310, 982
- Suntzeff, N. B., Schommer, R. A., Olszewski, E. W., & Walker, A. R. 1992, *AJ*, 104, 1743

- Suntzeff, N. B., Mateo, M., Terndrup, D. M., Olszewski, E. W., Geisler, D., & Weller, W. 1993, *ApJ*, 418, 208
- Tautvaisiene, G., Edvardsson, B., Puzeras, E., & Ilyin, I. 2005, *A&A*, 431, 933
- Tonry, J., & Davis, M. 1979, *AJ*, 84, 1511
- Twarog, B. A., Ashman, K. M., Anthony-Twarog, B. J. 1997, *AJ*, 114, 2556
- Valdes, F. 1992, Guide to the HYDRA Reduction task DOHYDRA
- Yong, D., Carney, B. W., & Teixeira de Almeida, M. L. 2005 *AJ*, 130, 597
- Zinn, R., & West, M. J. 1984 *ApJS*, 55, 45 (ZW84)
- Zoccali, M., Barbuy, B., Hill, V., Ortolani, S., Renzini, A., Bica, E., Monany, Y., Pasquini, L., Minniti, D., & Rich, R. M. 2004 *A&A*, 423, 507

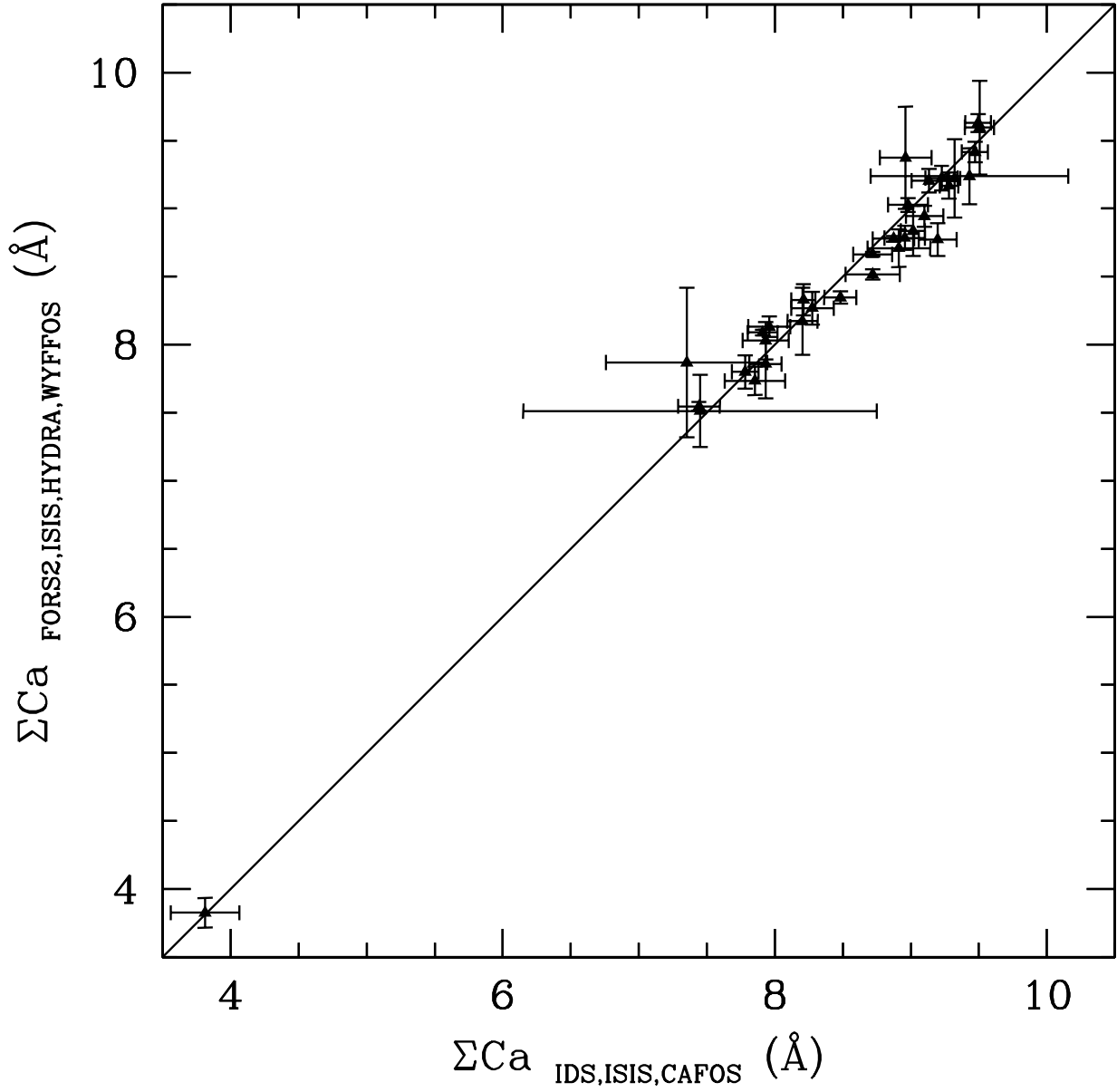


Fig. 1.— Comparison between equivalent widths for stars observed with different telescopes. Small differences are within the uncertainties.

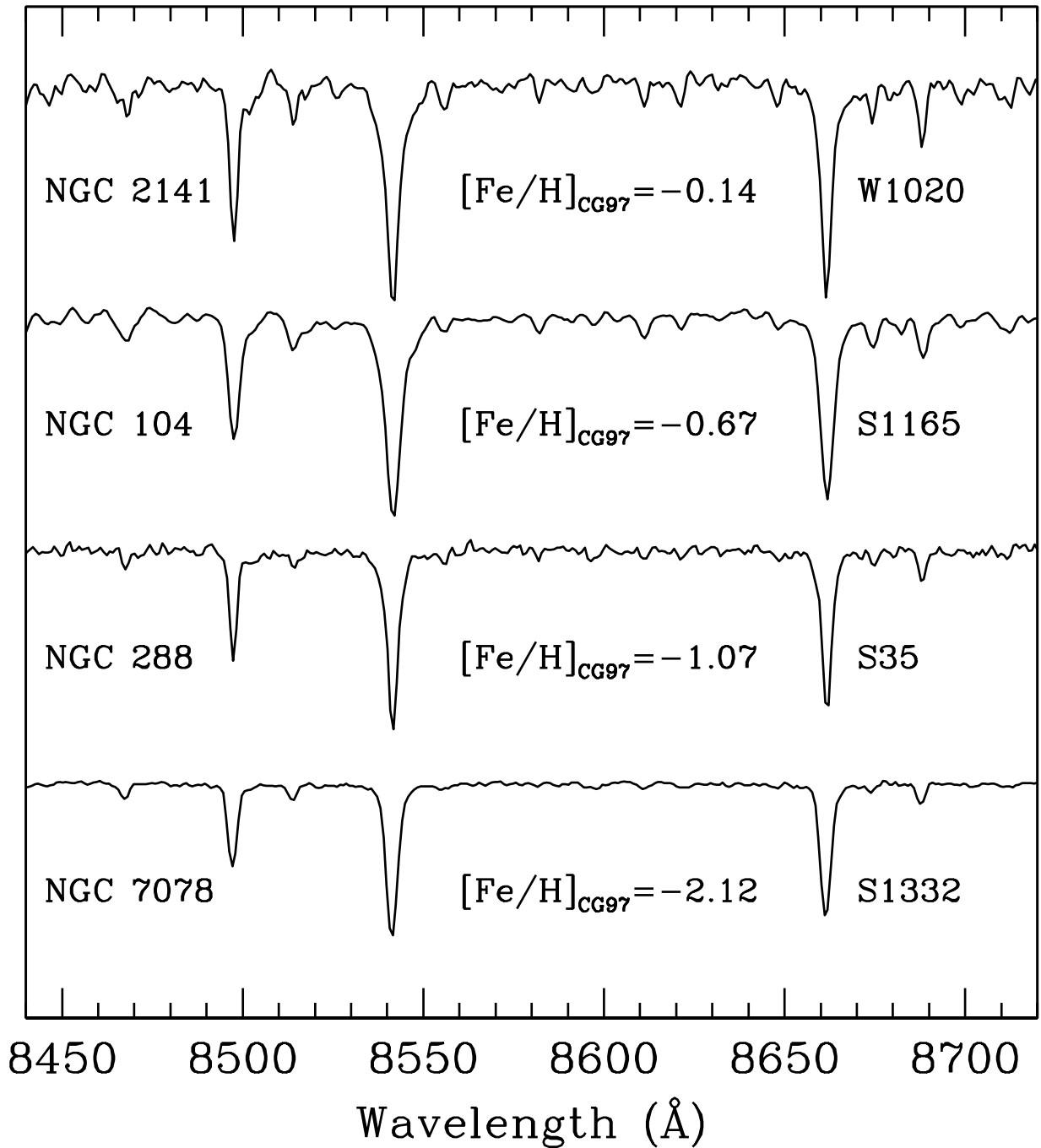


Fig. 2.— Spectra of four stars in clusters with different metallicities. The metallicity decreases from top to bottom. Note how the strength of the Ca II triplet lines increases with metallicity.

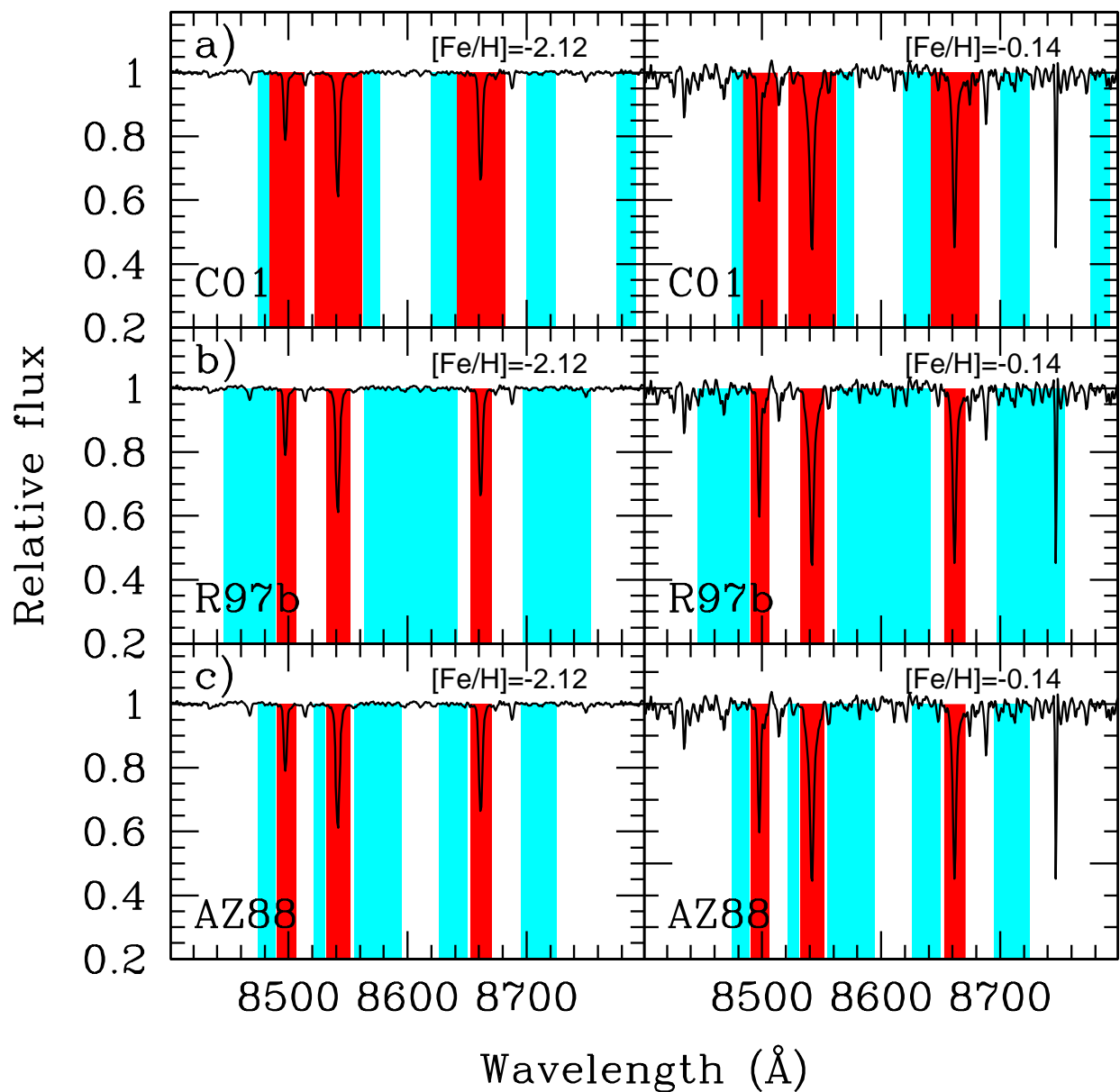


Fig. 3.— Continuum (clear) and line (dark) bandpasses defined by (a) Cenarro et al. (2001), (b) Rutledge et al. (1997a) and (c) Armandroff & Zinn (1988). They have been overplotted on to metal-poor (left) and metal-rich (right) stars. The bands of Cenarro et al. (2001) are wider in the lines to cover the wings fully and narrower in the continuum in order to avoid the most prominent molecular features for metal-rich stars.

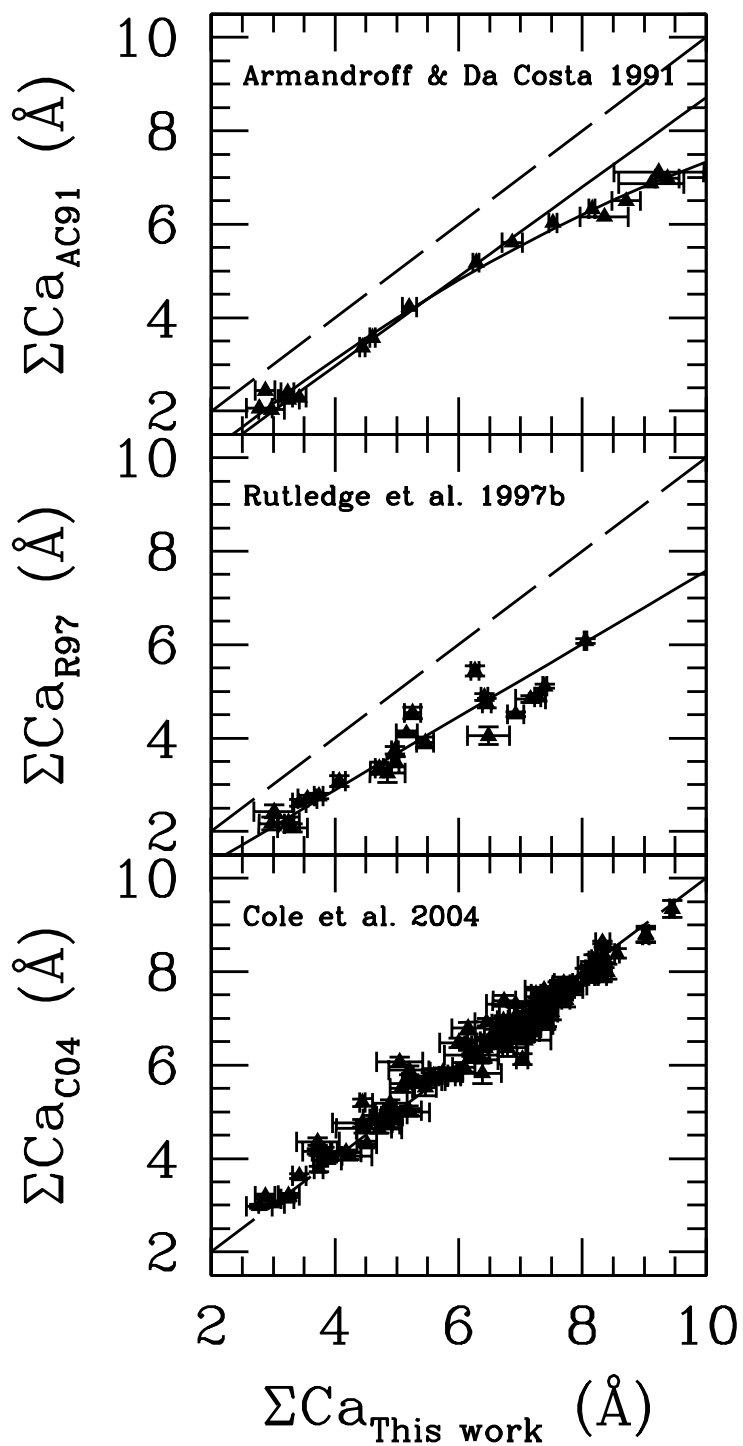


Fig. 4.— Comparison between ΣCa , as defined by Armandroff & Da Costa (1991), Rutledge et al. (1997b) and Cole et al. (2004), and the values obtained in this paper. The dashed lines represent the one-to-one equivalence. Solid lines are best fits to the data.

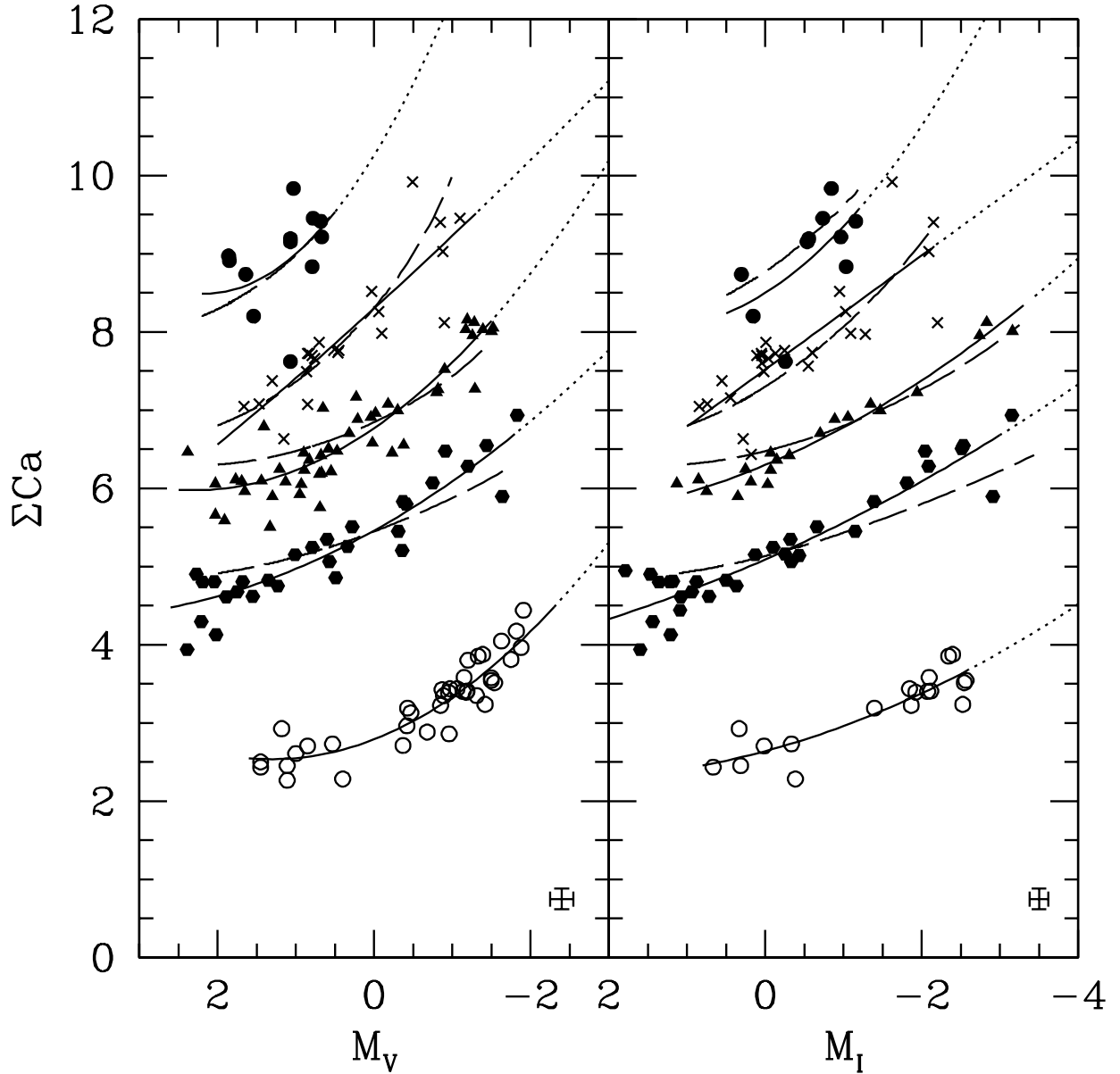


Fig. 5.— Stars in the M_V - ΣCa and M_I - ΣCa planes for the clusters in which we have observed stars along the RGB: NGC 7078 (open circles), NGC 288 (hexagons), NGC 104 (triangles), NGC 2141 (crosses) and NGC 6791 (filled circles). The individual quadratic fit to each cluster is plotted (solid lines). Dotted lines represent the extrapolation of the fit in the magnitude range where there are no calibration stars. We also plotted the theoretical predictions for each of them (dashed lines). The models have been shifted to match approximately the cluster sequences (see text for details). Errorbars are omitted for clarity, but the typical error is shown on the lower right corner.

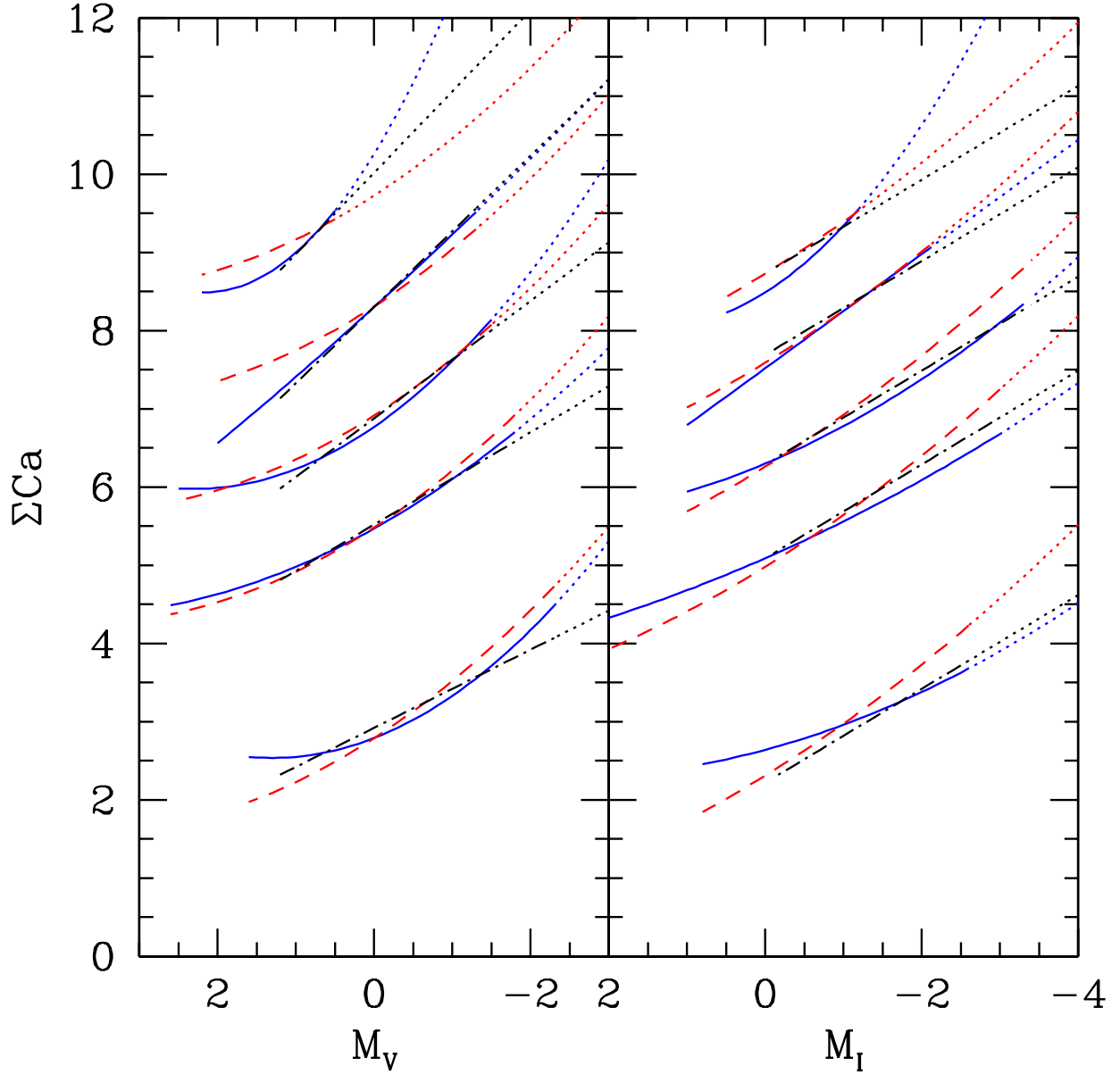


Fig. 6.— Different fits to the sequences of the clusters in which we have observed stars along the RGB in the M_V - ΣCa and M_I - ΣCa planes. Solid lines are the quadratic fit to each cluster independently. Dashed lines are the quadratic fit when the linear and quadratic terms are the same for all clusters. Finally, dotted-dashed lines are the linear fits for stars brighter than $M_V \leq 1.25$ and $M_I \leq 0$, assuming the same slope for all clusters. Dotted lines are the regions in which the fits are extrapolated.

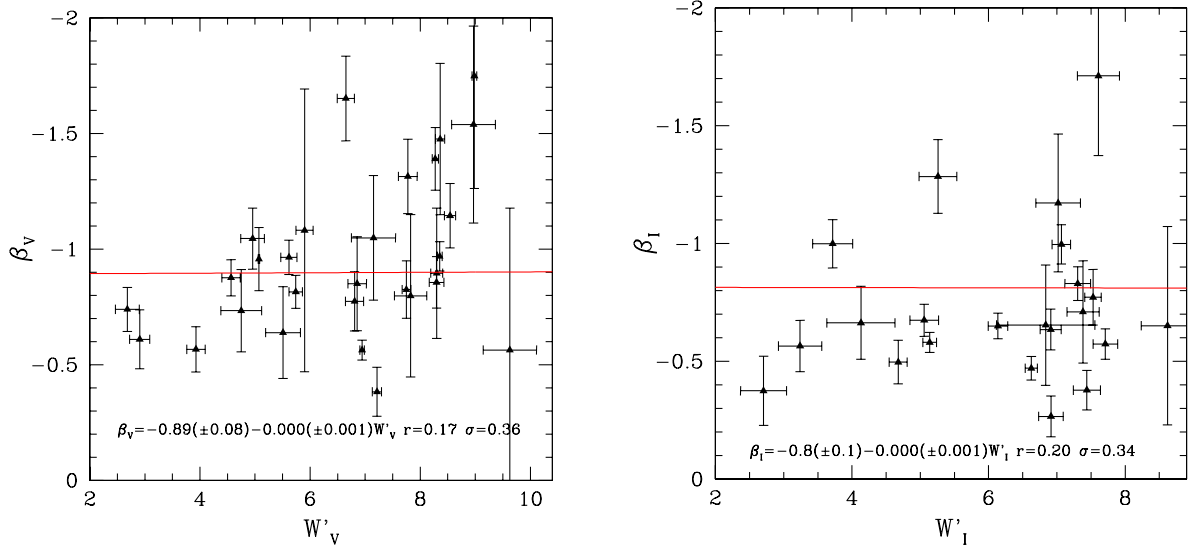


Fig. 7.— Values of the slopes obtained from the individual fit for each cluster, versus W' . Solid lines are the linear fit, which is given at the bottom. Note that there is no correlation between slope and W' (and therefore $[\text{Fe}/\text{H}]$) in any of the filters.

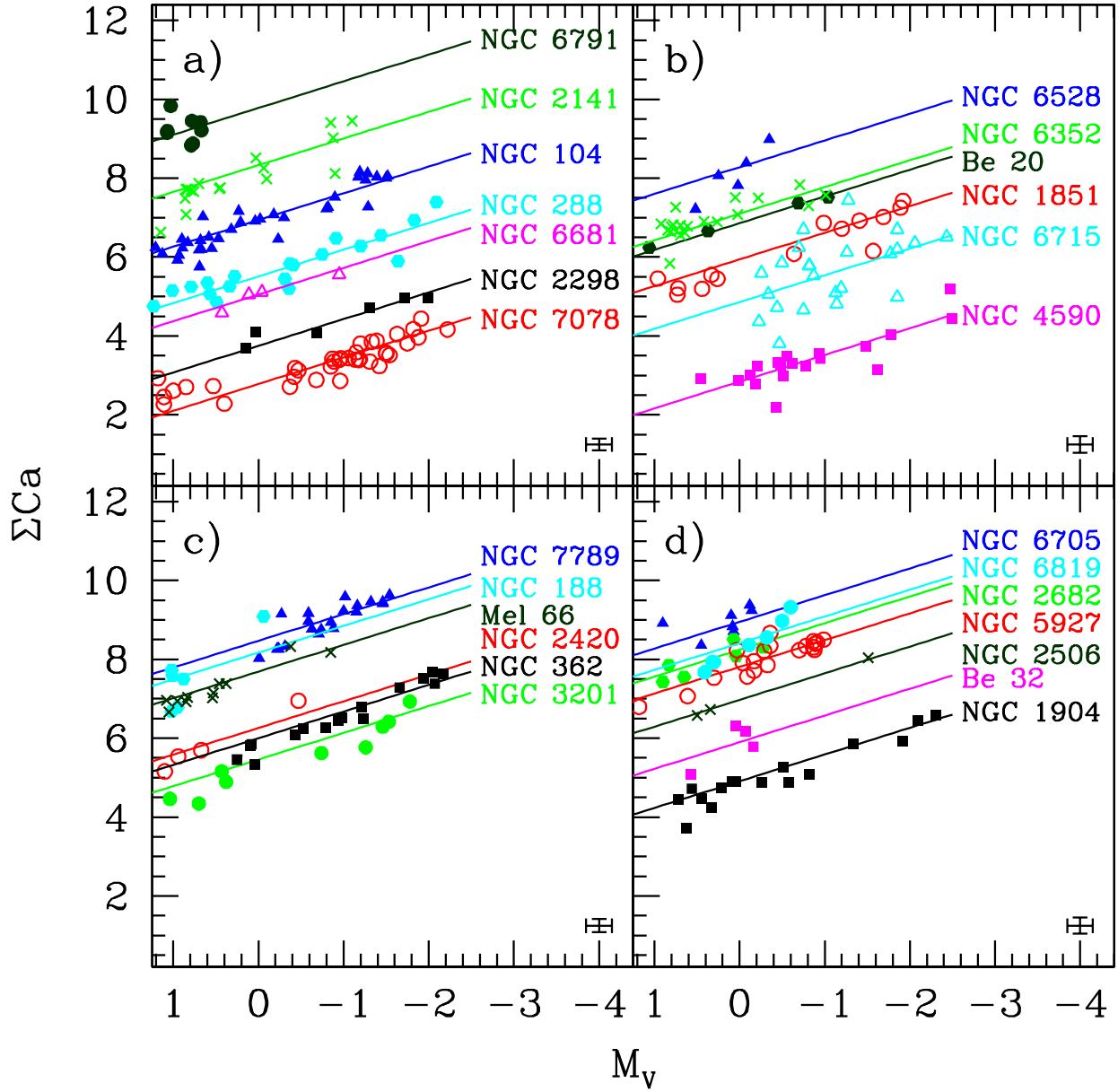


Fig. 8.— Cluster sample in the M_V - ΣCa plane. Solid lines are the linear fit to the stars in each cluster when we assume that the slope is the same for all of them. The typical error is shown on the lower right corner.

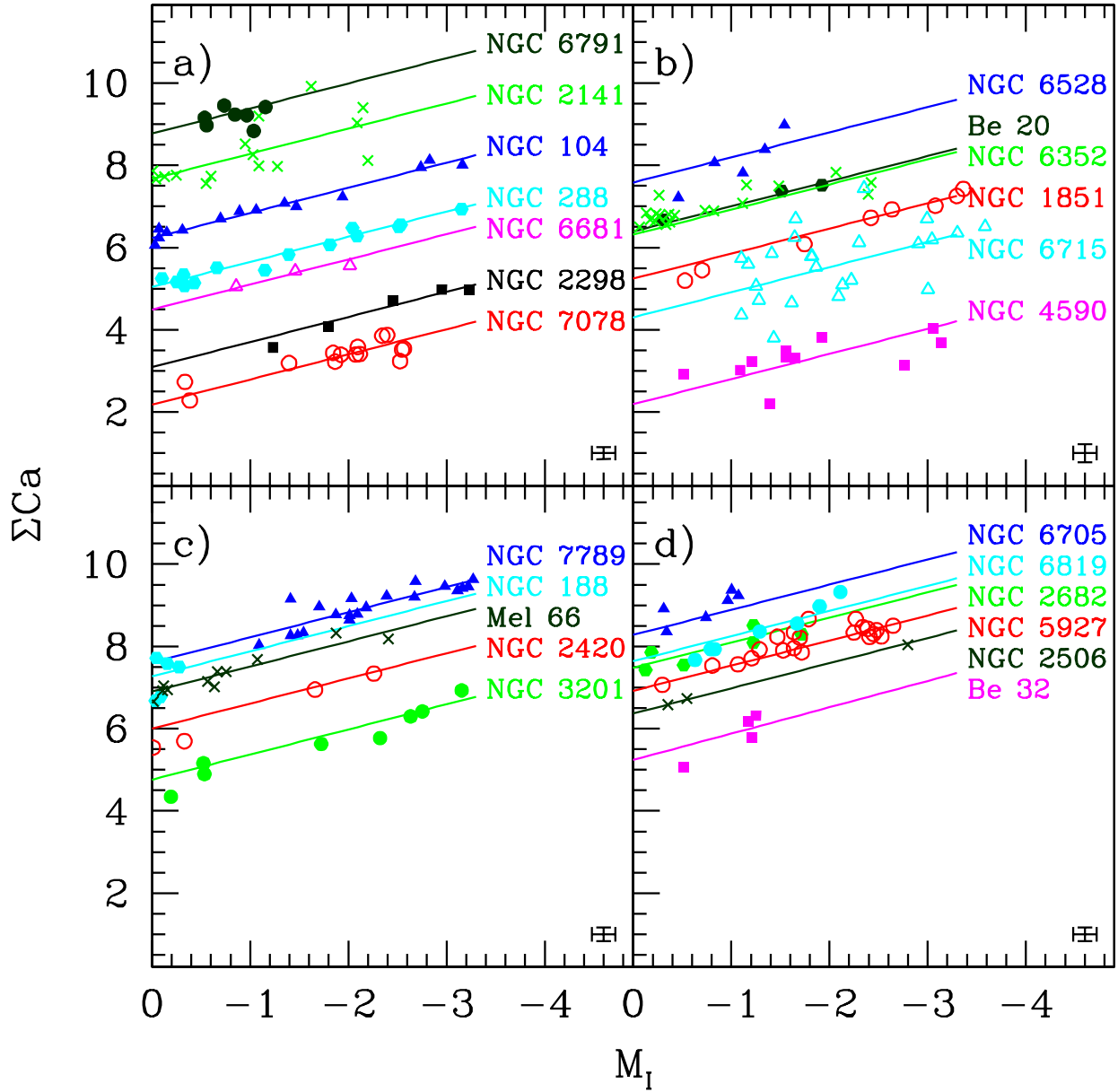


Fig. 9.— Same as Figure 8 but in the M_I - ΣCa plane.

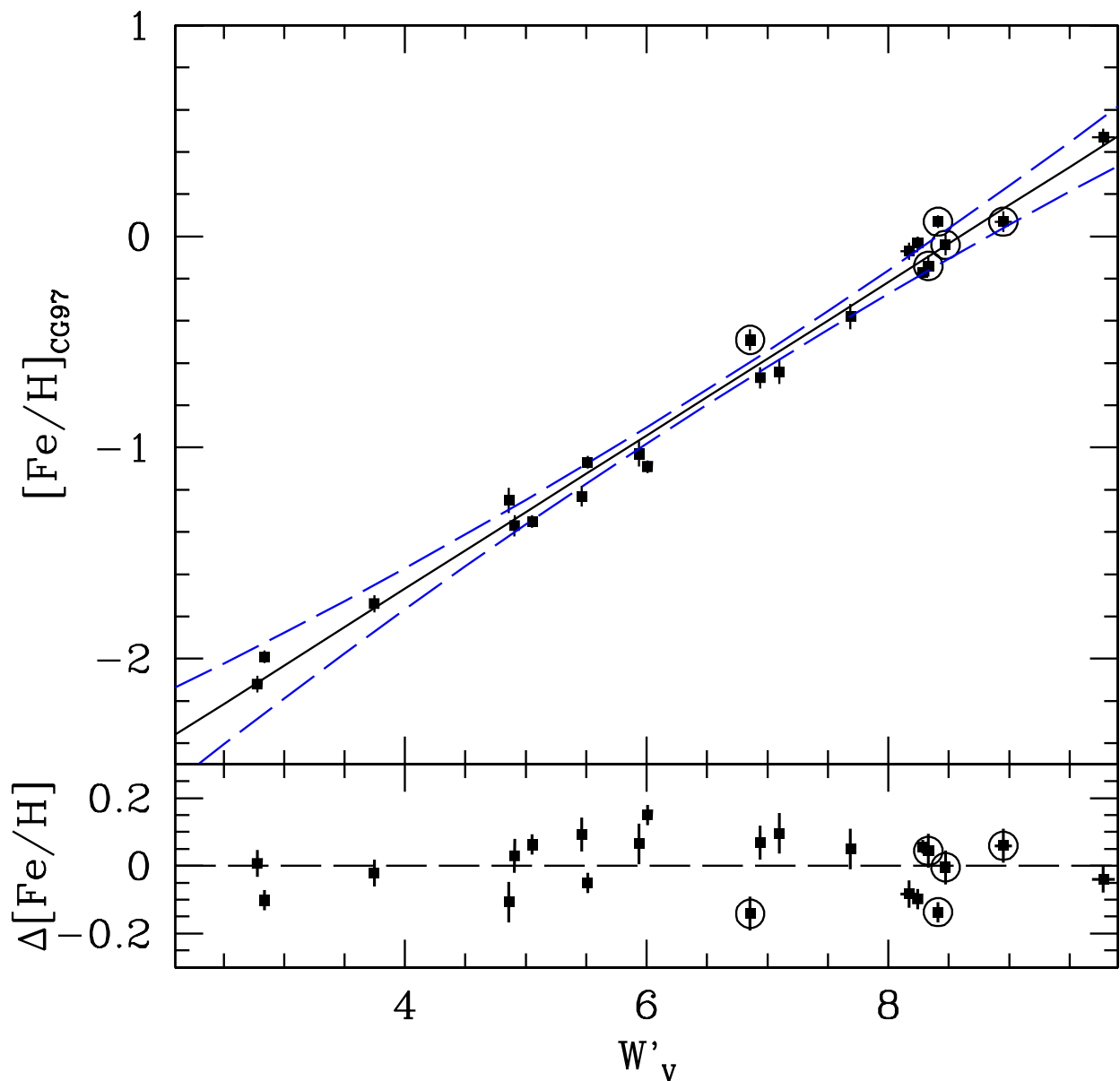


Fig. 10.— Top panel: $[\text{Fe}/\text{H}]$ versus W'_v . The solid lines are the best linear fit to the data. Dashed lines define the confidence band of the fit. Open circles are clusters younger than 4 Gyr. The residuals of the linear fit are shown in the bottom panel. Note that the W'_v errors are smaller than the size of points in most cases. The clusters excluded from the analysis (NGC 2420, NGC 2506 and Berkeley 32) have not been plotted.

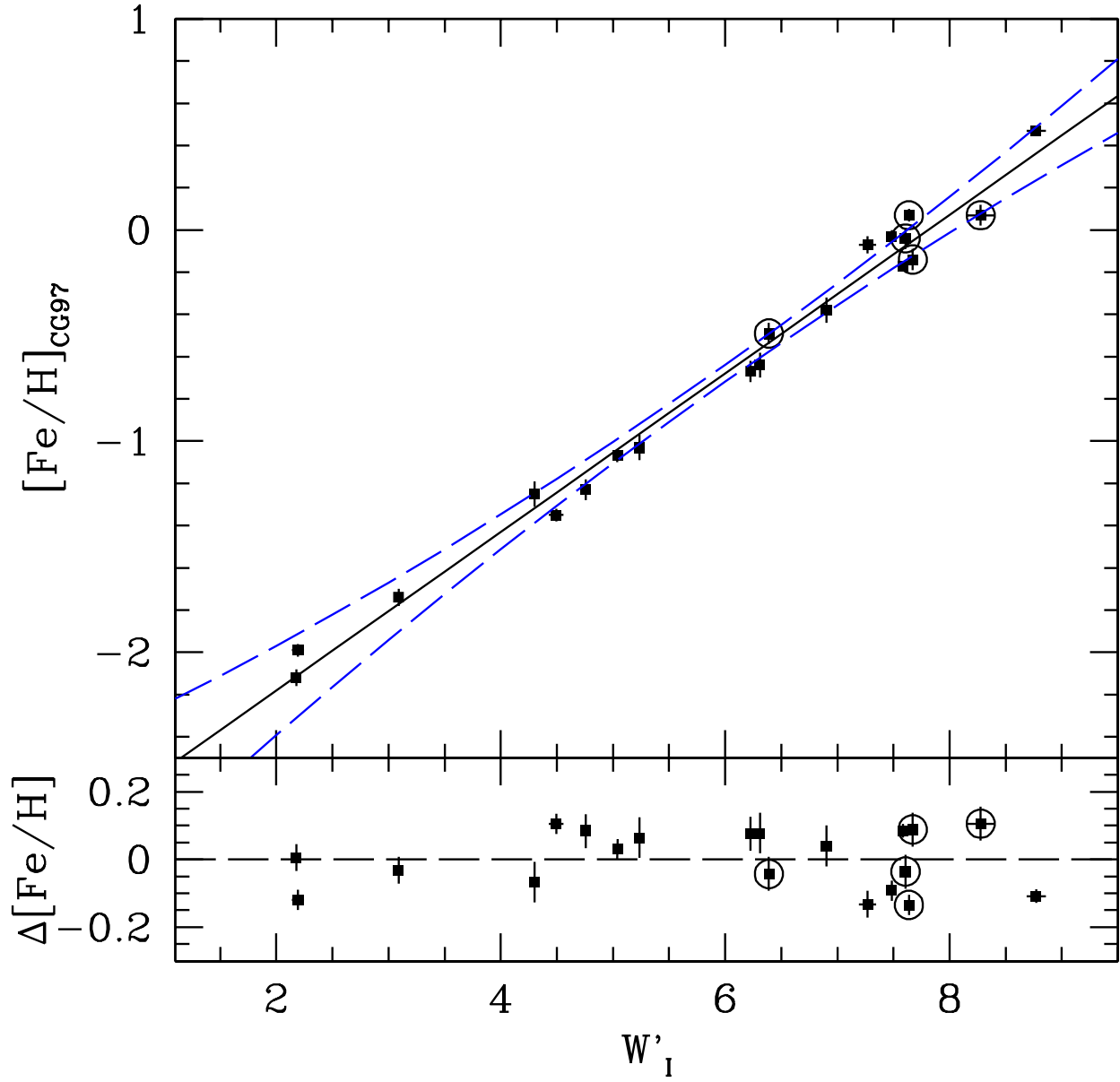


Fig. 11.— Same as Figure 10 but with W'_I .

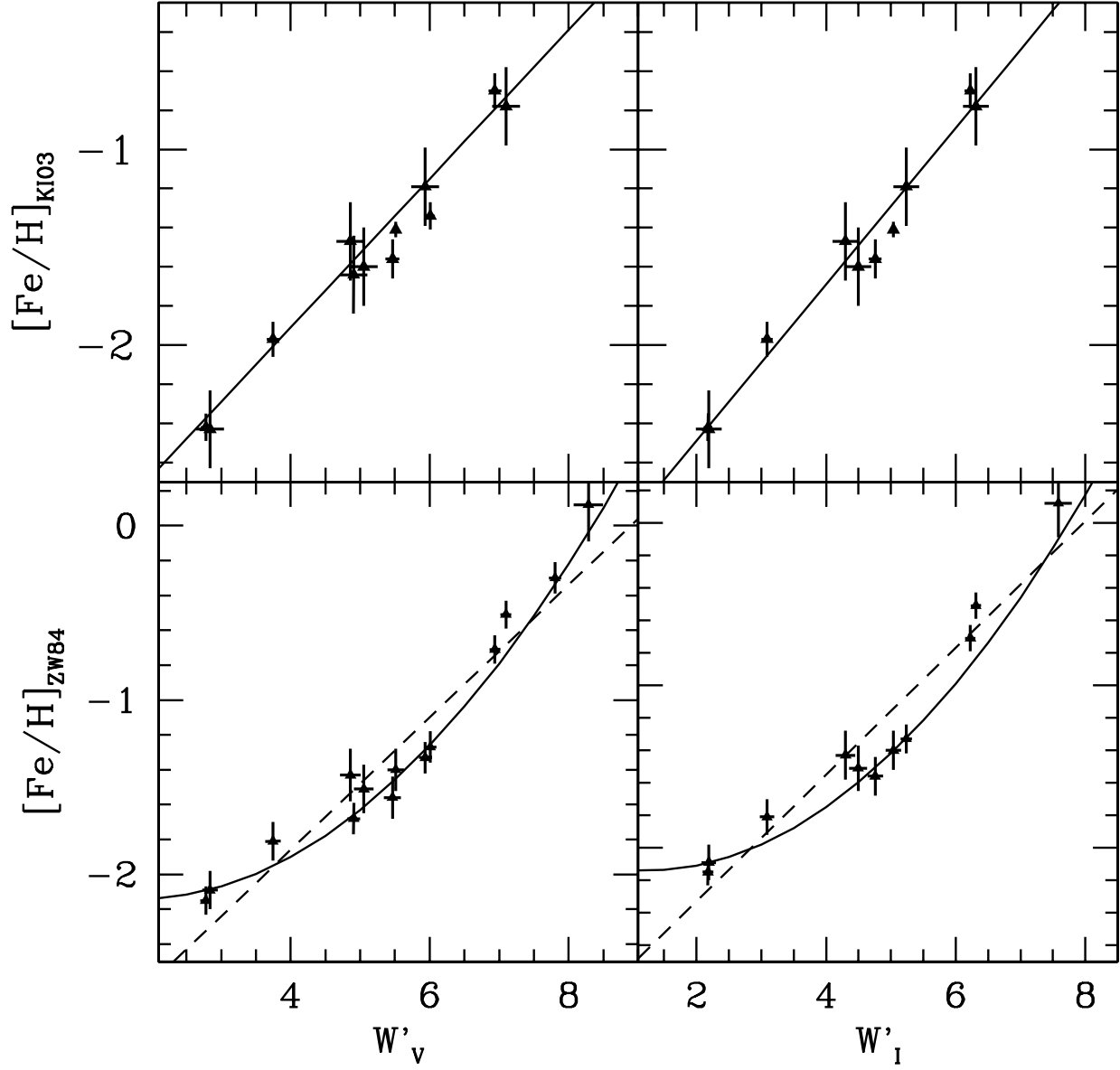


Fig. 12.— W'_v (left) and W'_I (right) versus $[\text{Fe}/\text{H}]$ on the KI03 (top) and the ZW84 (bottom) metallicity scales. The lines are the best fit to the data. In the case of the ZW84 metallicity scale, a second-order polynomial results in an improvement of the fit.

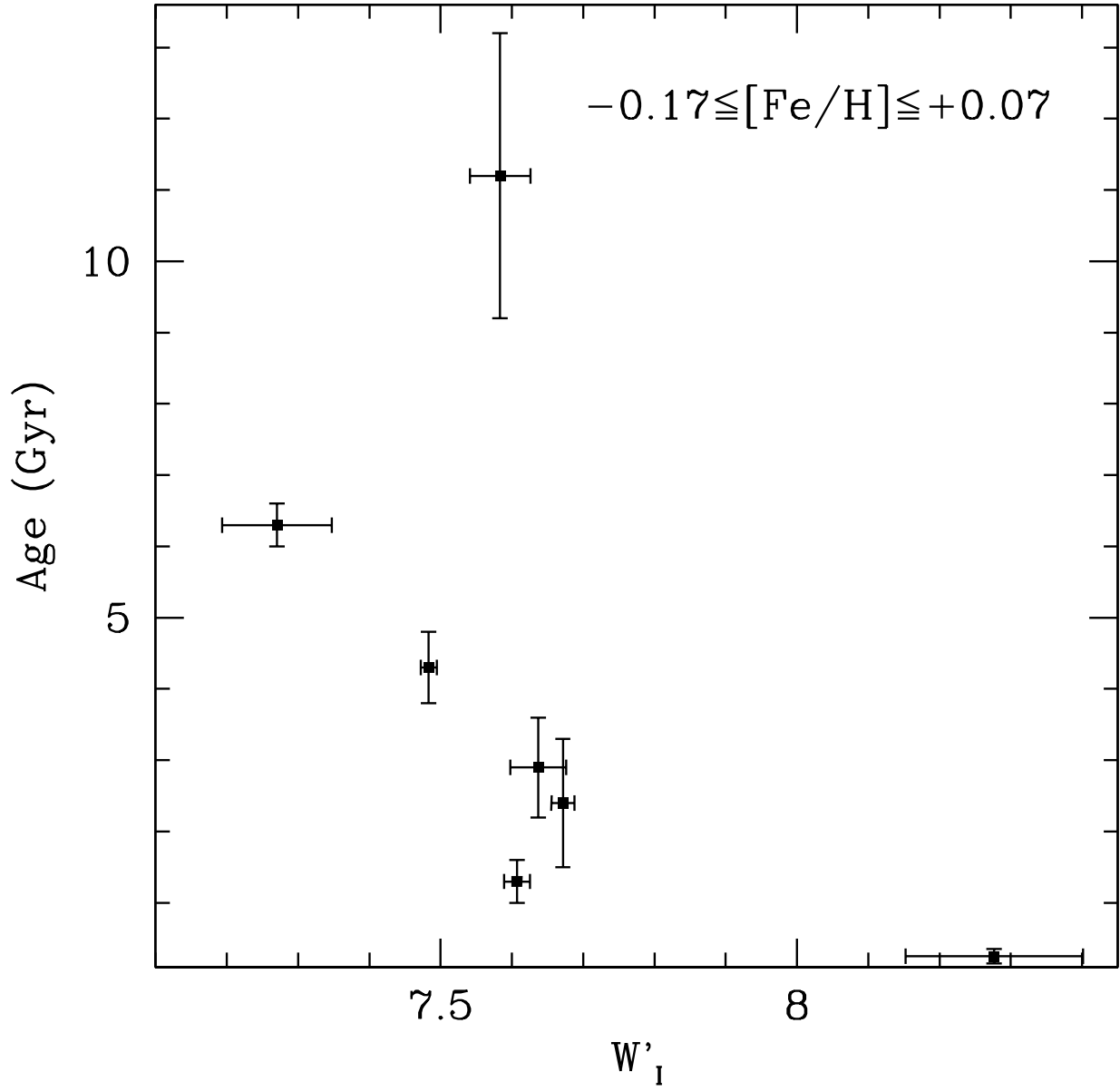


Fig. 13.— W'_I versus age for clusters with $-0.17 \leq [\text{Fe}/\text{H}] \leq +0.07$. Independently of their ages, all clusters have similar W'_I , with the exception of the youngest cluster, NGC 6705 (0.25 Gyr).

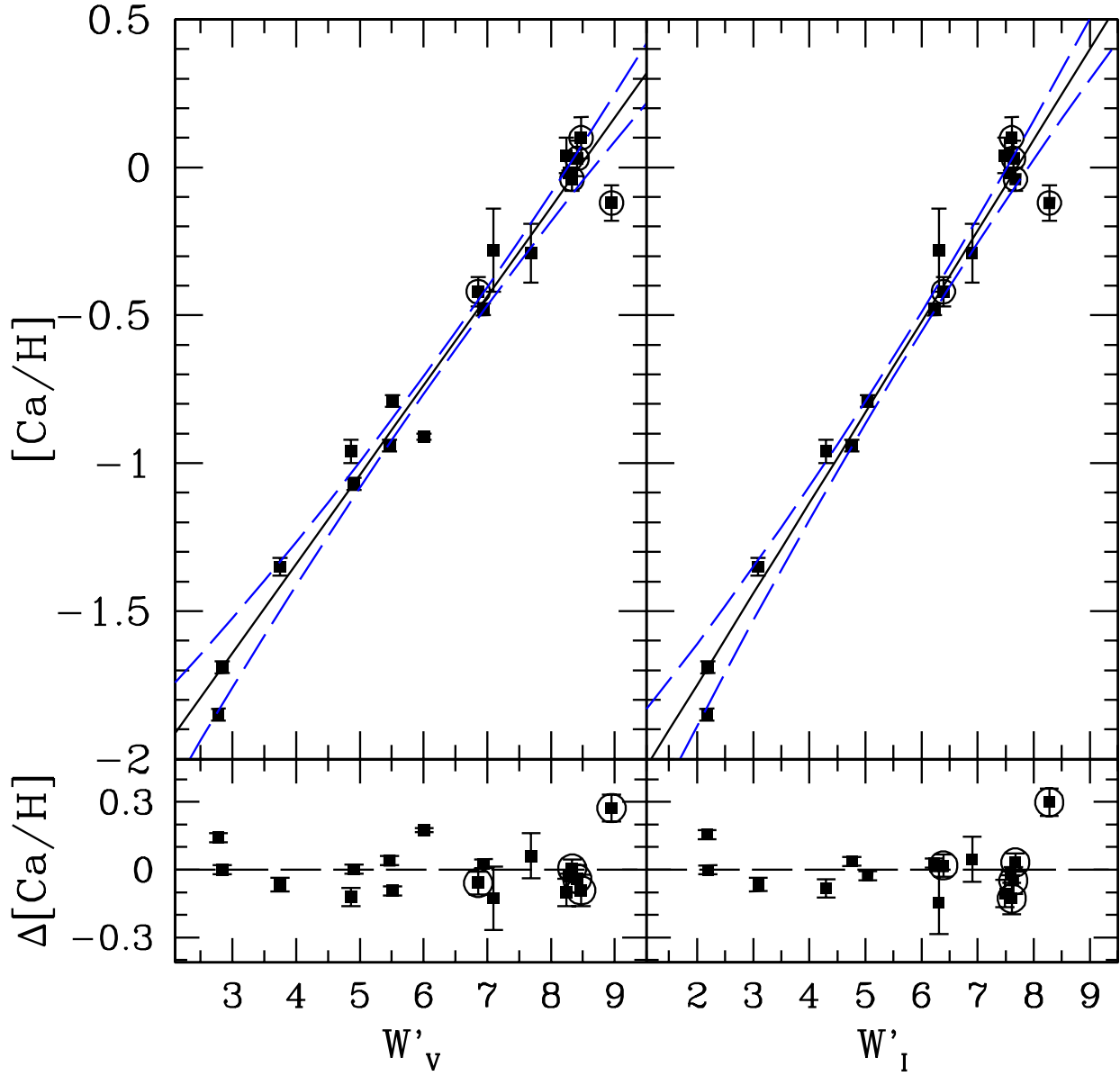


Fig. 15.— W'_V (left) and W'_I (right) versus $[Ca/H]$ ratio. The solid line is the best linear fit to the data. As before, open circles are clusters younger than 4 Gyr. The residuals of the linear fit are shown in the bottom panel.

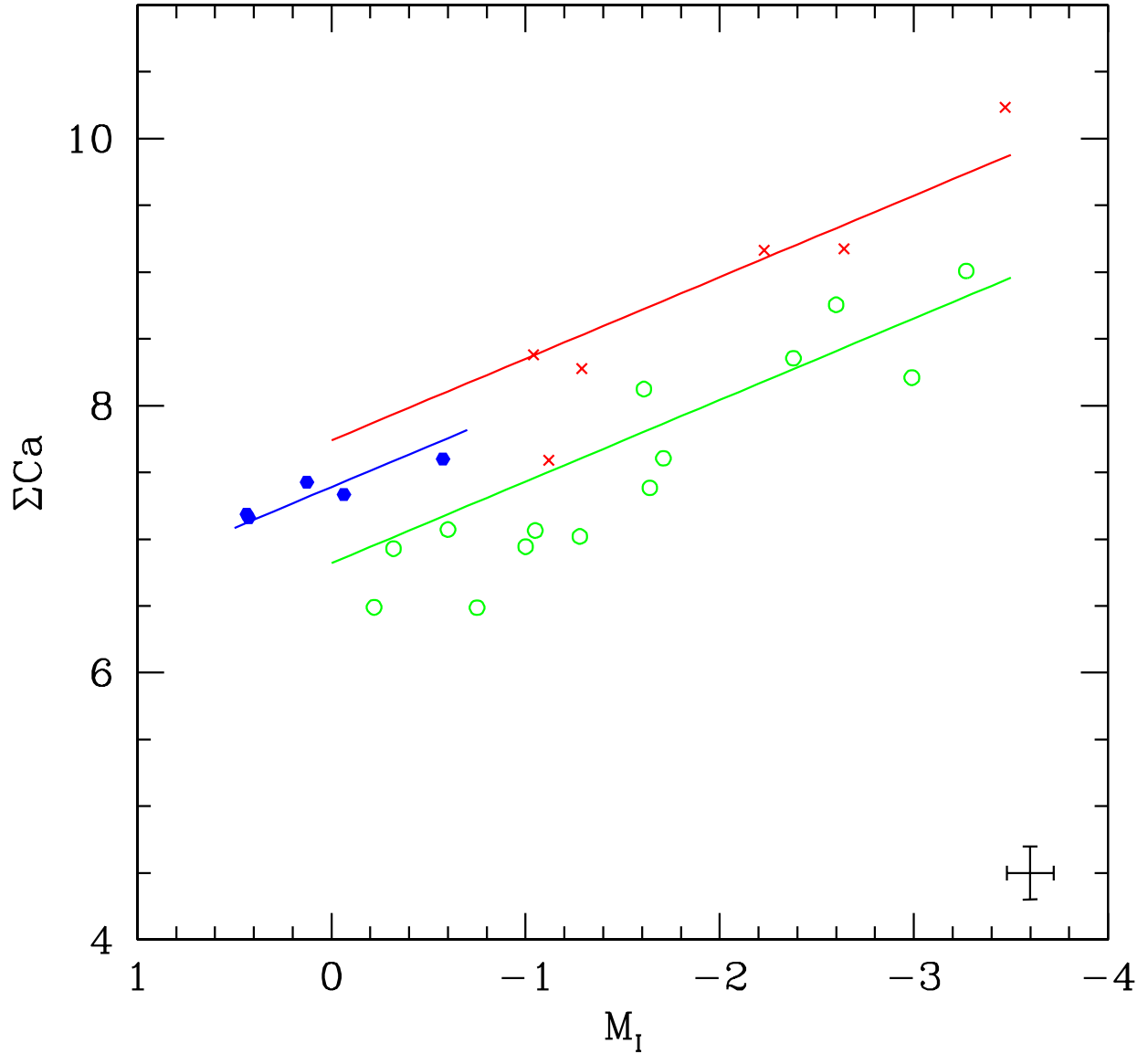


Fig. 16.— Sequences of clusters Berkeley 39 (hexagons), Trumpler 5 (open circles) and Collinder 110 (filled squares) in the M_I - ΣCa plane. Solid lines are the linear sequence fits to the data for each cluster when the same slope is assumed for all clusters. The typical error is shown on the lower right corner.

Table 1. Cluster sample.

Cluster	[Fe/H] _{CG97}	Ref.	[Fe/H] _{ZW84}	[Fe/H] _{K103}	[Ca/H]	Ref.	Age(Gyr)	Ref.	$(m - M)_V$	$E(B - V)$	Ref.	Run
shetrone00 NGC 104 (47 Tuc)	-0.67 ± 0.03	31	-0.71	-0.70	0.47 ± 0.02	31	10.7 ± 1.0	8	13.32	0.05	13	7
NGC 188	-0.07 ± 0.04	2	6.30 ± 0.3	9	11.44	0.09	17	3
NGC 288	-1.07 ± 0.03	1	-1.40	-1.41	-0.79 ± 0.02	33	11.3 ± 1.1	8	14.64	0.03	13	7
NGC 362	-1.09 ± 0.03	1	-1.27	-1.34	-0.91 ± 0.01	33	8.7 ± 1.5	8	14.75	0.05	13	7
NGC 1851	-1.36	9.2 ± 1.5	8	15.49	0.02	13	7
NGC 1904 (M79)	-1.37 ± 0.05	1	-1.69	-1.64	-1.07 ± 0.02	32	11.7 ± 1.3	8	15.53	0.01	13	7
Berkeley 20	-0.49 ± 0.05	22	-0.42 ± 0.05	22	4.05 ± 0.7	9	15.84	0.38	22	7
NGC 2141	-0.14 ± 0.05	22	-0.04 ± 0.04	22	2.45 ± 0.9	9	14.15	0.40	14	3,7
Collinder 110	1.3 ± 0.2	24	13.04	0.40	24	3
Trumpler 5	5.7 ± 2.3	9	14.50	0.60	23	3,7
NGC 2298	-1.74 ± 0.04	1	-1.85	-1.64	-1.35 ± 0.03	35	12.6 ± 1.4	8	15.54	0.13	13	7
Berkeley 32	-0.29 ± 0.04	32	5.9 ± 1.6	9	12.85	0.08	25	3
Melote 66	-0.38 ± 0.06	3	-0.29 ± 0.10	40	5.3 ± 1.4	9	13.63	0.14	26	7
Berkeley 39	7.0 ± 1.0	9	13.24	0.11	26	7
NGC 2420	-0.44 ± 0.15	3	2.2 ± 0.3	9	12.0	0.05	15	3
NGC 2506	-0.20 ± 0.01	31	2.1 ± 0.3	9	12.60	0.09	16	3,7
NGC 2682 (M 67)	-0.03 ± 0.03	4	$+0.01 \pm 0.06$	4	4.3 ± 0.5	9	9.65	0.04	17	3,7
NGC 3201	-1.24 ± 0.12	1	-1.61	-1.48	-1.11 ± 0.02	34	11.3 ± 1.1	8	14.17	0.21	13	4
NGC 4590 (M 68)	-2.00 ± 0.03	1	-2.09	-2.43	-1.68 ± 0.02	34	11.2 ± 0.9	8	15.14	0.04	13	3,4,6,7
NGC 5927	-0.30	10.9 ± 2.2	30	15.81	0.47	13	6
NGC 6352	-0.64 ± 0.02	1	-0.51	...	-0.63 ± 0.14	36	9.9 ± 1.4	8	14.39	0.21	13	6
NGC 6528	-0.17 ± 0.02	28,29	+0.12	...	-0.03 ± 0.01	37	11.2 ± 2.0	10	16.16	0.55	18	7
NGC 6681 (M 70)	-1.35 ± 0.03	1	-1.51	11.5 ± 1.4	8	14.93	0.07	13	7
NGC 6705 (M 11)	$+0.07 \pm 0.05$	5	-0.12 ± 0.06	5	0.25 ± 0.1	11	12.88	0.43	11	2,5
NGC 6715 (M 54)	-1.42	-1.47	-0.98 ± 0.04	39	12 ± 1.5	27	17.77	0.16	19	7
NGC 6791	$+0.47 \pm 0.04$	6	12.0 ± 1.0	12	13.07	0.09	12	5
NGC 6819	$+0.07 \pm 0.03$	7	$+0.03 \pm 0.06$	7	2.9 ± 0.7	9	12.35	0.14	20,7	1,5
NGC 7078 (M 15)	-2.12 ± 0.04	1	-2.15	-2.42	-1.88 ± 0.02	38	11.7 ± 0.8	8	15.31	0.09	13	7
NGC 7789	-0.04 ± 0.05	4	$+0.10 \pm 0.08$	4	1.3 ± 0.3	9	12.20	0.28	4,21	1,3

References. — (1) Carretta & Gratton (1997); (2) Hubbs et al. (1990); (3) Gratton (2000) (4) Tautvaisiene et al. (2005); (5) Gonzalez & Wallerstein (2000); (6) Gratton et al. (2006); (7) Bragaglia et al. (2001); (8) Salaris & Weiss (2002); (9) Salaris et al. (2004); (10) Feltzing & Johnson (2002); (11) Sung et al. (1999); (12) Stetson et al. (2003); (13) Rosenberg et al. (1999); (14) Carraro et al. (2001); (15) Lee et al. (1999); (16) Marconi et al. (1997); (17) Sarajedini et al. (1999); (18) Ortolani et al. (1992); (19) Rosenberg et al. (2004); (20) Rosvick & Vandenberg (1998); (21) Gim et al. (1998); (22) Yong et al. (2005); (23) Kim & Sung (2003); (24) Bragaglia & Tosi (2003); (25) Richtler & Sagar (2001);

(26) Kassis et al. (1997); (27) Layden & Sarajedini (1997) (28) Zoccali et al. (2004); (29) Origlia et al. (2005); (30) Fullton (1996); (31) Carretta et al. (2004); (32) Sestito et al. (2006); (33) Shetrone & Keane (2000); (34) Gratton & Ortolami (1989); (35) McWilliam et al. (1992); (36) Gratton (1987); (37) Carretta et al. (2001); (38) Sneden et al. (1997); (39) Brown et al. (1999); (40) Gratton & Contarini (1994).

Table 2. Observing runs

Run	Date	Telescope	Instrument	Resolution	Å/pix
1	May 2002	WHT	ISIS	7000	0.41
2	April 2002	WHT	WYFFOS	4000	1.5
3	December 2002	INT	IDS	6000	0.45
4	January 2005	CTIO 4m	HYDRA	6000	0.9
5	June 2005	CAHA 2.2m	CAFOS	2000	2.0
6	2005	VLT	FORS2 MXU	5000	0.85
7	ESO Archive	VLT	FORS2 MXU/MOS	5000	0.85

Table 3. Star sample.

Cluster	Id	ΣCa	$\sigma_{\Sigma\text{Ca}}$	V	I	V_r	σ_{V_r}	Comments
ngc104	S2701	6.18	0.13	14.07	99.99	2.22	4.90	Member?
ngc104	S2703	6.55	0.07	12.99	99.99	4.44	4.34	No member
ngc104	S2705	7.27	0.02	12.08	99.99	-13.24	3.68	
ngc104	S2707	6.96	0.07	13.35	99.99	-2.71	5.46	
ngc104	S2712	7.34	0.05	12.89	99.99	9.46	5.25	No member

References. — **NGC 104** Lee (1977) [L], Stetson (2000) [S]; **NGC 188** Webda <http://obswww.unige.ch/webda/> (Mermilliod 1995) [W]; **NGC 288** Alcaino & Liller (1980) [A]; **NGC 362** Harris (1982) [H]; **NGC 1851** Stetson (1981) [S]; **NGC 1904** Stetson & Harris (1977) [S]; **Berkeley 20** Webda [W]; **NGC 2141** Burkhead et al. (1972) [B]; Rosvick (1995) [R]; Webda [W]; **Collinder 110** Webda [W]; **Trumpler 5** Webda [W]; **NGC 2298** Alcaino & Liller (1986) [A], Alcaino (1974) [A]; **Berkeley 32** Webda [W]; **Melotte 66** Webda [W]; **Berkeley 39** Webda [W]; **NGC 2420** Webda [W]; **NGC 2506** Webda [W]; **NGC 2682** Webda [W]; **NGC 3201** Stetson (2000) [S]; **NGC 4590** Harris (1975a) [H], Stetson (2000) [S]; **NGC 5927** Zoccali (private communication); **NGC 6352** Zoccali (private communication); **NGC 6528** Ortolani et al. (1992) [O]; **NGC 6681** Harris (1975b) [H] Rosenberg et al. (2000) [R]; **NGC 6705** Sung et al. (1999) [S]; **NGC 6715** Rosenberg et al. (2004) [R]; **NGC 6791** Stetson et al. (2003) [S]; **NGC 6819** Webda [W]; **NGC 7078** Buonanno et al. (1983) [B]; Stetson (2000) [S]; **NGC 7789** Webda [W];

Note. — Table 3 is published in its entirety in the electronic edition of *Astronomical Journal*. A portion is shown here for guidance regarding its form and content.

Table 4. Radial velocities of the cluster sample.

Cluster	V_r	$\sigma(V_r)$	Stars	V_r (ref.)	Ref.
NGC 104 (47 Tuc)	-16	11	32	-18.7	1
NGC 188	-44	20	8	-45	2
NGC 288	-50	11	19	-46.6	1
NGC 362	213	7	16	223.5	1
NGC 1851	321	9	14	320.5	1
NGC 1904 (M79)	227	5	16	206	1
Berkeley 20	80	7	4	70	2
NGC 2141	44	10	21	33/64	3,4
Collinder 110	45	11	8
Trumpler 5	44	10	15	54	4
NGC 2298	153	15	6	148.9	1
Berkeley 32	98	12	3	101	2
Melote 66	18	10	11	23	5
Berkeley 39	59	6	5	55	2
NGC 2420	69	5	5	67	2
NGC 2506	76	5	3	84	6
NGC 2682 (M 67)	36	6	9	33	2
NGC 3201	491	3	10	494	1
NGC 4590 (M 68)	-89	7	19	-93.4	1
NGC 5927	-84	5	20	-107.5	1
NGC 6352	-114	8	23	-121	1
NGC 6528	220	7	5	206	1
NGC 6681 (M 70)	199	7	4	220	1
NGC 6705 (M 11)	28	7	10	34	7
NGC 6715 (M 54)	156	8	23	142	1
NGC 6791	-46	10	10	-57	2
NGC 6819	2	5	7	-5	2
NGC 7078 (M 15)	-108	10	33	-107	1
NGC 7789	-58	6	20	-64	2

References. — (1) Harris (1996); (2) Friel et al. (2002); (3) Friel (1989); (4) Cole et al. (2004) (5) Friel & Janes (1993); (6) Mathieu (1985); (7) Mathieu et al. (1986)

Table 5. Line and continuum bandpasses

Line Bandpasses (\AA)	Continuum bandpasses (\AA)
8484-8513	8474-8484
8522-8562	8563-8577
8642-8682	8619-8642
...	8799-8725
...	8776-8792

Table 6. Coefficients of the quadratic fits in the form $\Sigma Ca = W' + \beta M_{V,I} + \gamma M_{V,I}^2$ to the sequence of each cluster individually. The clusters are ordered by metallicity.

Cluster	W'	β	γ	σ
		M_V		
NGC 6791	10.26±0.97	-1.64±1.28	0.38±0.35	0.72
NGC 2141	8.30±0.14	-0.91±0.13	0.02±0.15	0.44
NGC 104	6.77±0.06	-0.69±0.05	0.15±0.04	0.30
NGC 288	5.46±0.08	-0.56±0.05	0.07±0.03	0.29
NGC 7078	2.79±0.06	-0.39±0.04	0.15±0.04	0.22
		M_I		
NGC 6791	8.49±0.24	-0.63±0.74	0.22±0.79	0.54
NGC 2141	7.52±0.11	-0.73±0.20	0.00±0.11	0.47
NGC 104	6.30±0.04	-0.42±0.05	0.06±0.02	0.14
NGC 288	5.09±0.07	-0.44±0.04	0.03±0.03	0.27
NGC 7078	2.64±0.08	-0.27±0.14	0.05±0.07	0.22

Table 7. Derived W'_V and W'_I and number of stars used.

Cluster	W'_V	#Star	W'_I	#Star
NGC 104	6.94 ± 0.01	34	6.23 ± 0.01	14
NGC 188	8.17 ± 0.07	6	7.27 ± 0.08	5
NGC 288	5.51 ± 0.01	19	5.04 ± 0.03	14
NGC 362	6.01 ± 0.01	16
NGC 1851	5.94 ± 0.03	14	5.24 ± 0.04	8
NGC 1904	4.91 ± 0.03	16
Berkeley 20	6.86 ± 0.03	4	6.39 ± 0.03	3
NGC 2141	8.33 ± 0.01	18	7.67 ± 0.02	15
Collinder 110	8.21 ± 0.04	11	7.74 ± 0.06	6
Trumpler 5	7.52 ± 0.04	16	6.97 ± 0.04	15
NGC 2298	3.75 ± 0.03	6	3.09 ± 0.03	5
Berkeley 32	5.90 ± 0.08	4	5.27 ± 0.08	4
Melote 66	7.69 ± 0.03	11	6.90 ± 0.03	11
Berkeley 39	8.21 ± 0.04	5	7.27 ± 0.06	3
NGC 2420	6.26 ± 0.09	6	6.15 ± 0.08	4
NGC 2506	6.96 ± 0.09	4	6.37 ± 0.09	3
NGC 2682	8.24 ± 0.01	6	7.48 ± 0.01	8
NGC 3201	5.46 ± 0.03	9	4.76 ± 0.02	6
NGC 4590	2.84 ± 0.02	19	2.19 ± 0.06	12
NGC 5927	7.81 ± 0.01	21	6.92 ± 0.01	13
NGC 6352	7.10 ± 0.01	19	6.31 ± 0.01	19
NGC 6528	8.28 ± 0.04	5	7.58 ± 0.04	5
NGC 6681	5.05 ± 0.03	4	4.49 ± 0.07	3
NGC 6705	8.95 ± 0.07	7	8.28 ± 0.12	6
NGC 6715	4.86 ± 0.03	23	4.30 ± 0.03	24
NGC 6791	9.78 ± 0.09	9	8.77 ± 0.09	8
NGC 6819	8.41 ± 0.04	7	7.64 ± 0.04	7
NGC 7078	2.78 ± 0.01	38	2.18 ± 0.01	14
NGC 7789	8.47 ± 0.02	20	7.61 ± 0.02	20

Table 1. Star sample.

Cluster	Id	ΣCa	$\sigma_{\Sigma\text{Ca}}$	V	I	V-r	σ_{V_r}	Comments
NGC 104	L2701	6.19	0.13	14.07	...	2.2	4.9	Member?
NGC 104	L2703	6.55	0.07	12.99	...	4.4	4.3	Member?
NGC 104	L2705	7.27	0.02	12.08	...	-13.2	3.7	
NGC 104	L2707	6.96	0.07	13.35	...	-2.7	5.4	
NGC 104	L2712	7.34	0.05	12.89	...	9.4	5.2	No member
NGC 104	L2720	6.51	0.11	13.95	...	-30.7	5.4	
NGC 104	L2722	6.48	0.10	13.84	...	-1.6	5.1	
NGC 104	L2730	6.20	0.12	14.04	...	-6.2	3.4	
NGC 104	L3618	5.51	0.21	14.70	...	-11.1	5.3	
NGC 104	L3703	5.66	0.21	15.40	...	-5.8	4.1	
NGC 104	L3709	7.27	0.05	12.55	...	-20.4	4.7	
NGC 104	L3712	6.09	0.13	15.06	...	-28.1	5.6	
NGC 104	L3727	5.76	0.10	14.06	...	-25.9	5.6	
NGC 104	L3730	8.05	0.02	11.85	...	-29.3	3.8	
NGC 104	L3736	8.03	0.03	11.98	...	-22.8	4.1	
NGC 104	L3740	6.22	0.10	13.92	...	-26.4	6.4	
NGC 104	L3752	5.92	0.25	14.32	...	-28.9	3.7	
NGC 104	L5309	8.03	0.05	12.20	...	-20.8	8.2	
NGC 104	L5310	6.58	0.12	13.39	...	4.4	7.6	Member?
NGC 104	L5311	4.62	0.30	15.07	...	-9.9	6.2	
NGC 104	L5312	8.16	0.05	12.18	...	-17.4	9.4	

Table 1—Continued

Cluster	Id	ΣCa	$\sigma_{\Sigma\text{Ca}}$	V	I	V–r	σ_{V_r}	Comments
NGC 104	L5418	5.59	0.35	15.28	...	-30.6	7.3	
NGC 104	L5419	7.03	0.09	14.02	...	-26.9	8.5	
NGC 104	L5420	5.87	0.53	15.78	...	-104.4	5.7	No member
NGC 104	L5422	7.53	0.06	12.47	...	-29.2	7.8	
NGC 104	L5523	6.46	0.12	15.75	...	-4.7	7.7	
NGC 104	L5527	7.17	0.15	13.60	...	-23.9	7.4	
NGC 104	L5528	6.79	0.30	14.78	...	-5.1	7.1	
NGC 104	L5530	6.45	0.19	13.14	...	-25.8	7.6	
NGC 104	L6401	6.10	0.32	14.81	...	-25.0	7.1	
NGC 104	S1186	7.00	0.04	13.07	11.82	-18.1	3.0	
NGC 104	S2070	6.25	0.08	14.58	13.54	-11.1	3.4	L3735
NGC 104	S2069	6.08	0.11	14.50	13.47	-23.4	3.3	L3701
NGC 104	S2073	6.70	0.06	13.69	12.59	-9.3	3.0	
NGC 104	S1014	8.12	0.03	12.09	10.46	-20.1	2.3	L3708
NGC 104	S1024	3.70	0.09	14.78	13.73	8.1	1.3	L3707
NGC 104	S1096	6.88	0.05	13.58	12.40	-20.6	3.0	L3716
NGC 104	S2074	6.45	0.09	14.27	13.22	-18.0	3.2	
NGC 104	S2072	5.90	0.10	14.67	13.64	-20.0	2.9	
NGC 104	S1168	6.05	0.09	14.30	13.26	-32.4	3.3	
NGC 104	S1153	6.06	0.15	15.40	14.42	-2.7	3.5	
NGC 104	S1165	7.23	0.03	12.57	11.35	-21.3	2.9	

Table 1—Continued

Cluster	Id	ΣCa	$\sigma_{\Sigma\text{Ca}}$	V	I	V–r	σ_{V_r}	Comments
NGC 104	S1019	8.01	0.03	11.87	10.13	-23.2	0.1	L2620
NGC 104	S1054	6.11	0.15	15.14	14.14	-18.2	3.0	L2719
NGC 104	S1080	7.95	0.02	12.11	10.55	-21.0	0.1	L2721
NGC 104	S1048	6.23	0.10	14.26	13.22	-29.3	3.0	L2717
NGC 104	S1059	6.37	0.09	14.20	13.14	-15.9	3.0	L2714
NGC 104	S1193	6.42	0.08	14.05	12.98	-15.5	3.1	
NGC 104	S1111	5.96	0.12	15.02	14.04	-18.9	3.5	L2709
NGC 104	S1203	7.08	0.06	13.19	11.94	-17.3	3.4	
NGC 104	S1181	6.91	0.05	13.41	12.23	-19.8	3.2	
NGC 188	W1057	6.13	0.15	13.68	12.52	-54.4	5.7	
NGC 188	W1069	7.50	0.22	12.32	11.02	-63.7	6.0	
NGC 188	W1105	6.78	0.21	12.39	11.21	-63.5	6.0	
NGC 188	W2051	6.61	0.12	12.97	11.78	-63.1	6.8	
NGC 188	W2072	7.58	0.14	12.45	11.14	-65.4	6.5	
NGC 188	W2076	7.72	0.15	12.46	11.25	-59.1	8.2	
NGC 188	W3018	9.08	0.18	11.38	...	-65.6	7.0	
NGC 188	W5217	6.68	0.18	12.46	11.26	-62.7	6.1	
NGC 188	W7330	7.49	0.15	12.86	11.62	-64.4	6.7	
NGC 288	A0156	5.80	0.11	14.42	...	-57.7	2.4	
NGC 288	A0158	5.20	0.11	14.47	...	-53.8	6.2	
NGC 288	A0166	5.26	0.13	15.17	...	-65.2	5.5	

Table 1—Continued

Cluster	Id	ΣCa	$\sigma_{\Sigma\text{Ca}}$	V	I	V–r	σ_{V_r}	Comments
NGC 288	A0172	4.86	0.15	15.32	...	-60.4	4.7	
NGC 288	A0196	5.45	0.10	14.52	13.63	-69.2	5.6	
NGC 288	A0213	6.93	0.03	13.00	11.63	-69.5	6.0	
NGC 288	A0222	5.14	0.15	15.28	14.34	-70.2	5.5	
NGC 288	A0245	6.55	0.06	13.39	12.24	-53.9	4.8	
NGC 288	A0260	7.06	0.03	12.57	...	-71.4	4.4	
NGC 288	A0307	6.28	0.06	13.63	12.69	-56.7	5.3	
NGC 288	A0096	7.39	0.03	12.74	14.21	-57.7	1.6	
NGC 288	A0199	6.51	0.05	13.50	12.26	-71.2	5.9	
NGC 288	S0183	5.16	0.08	15.48	14.53	-20.9	3.4	A0181, No member
NGC 288	S0188	4.80	0.22	16.87	16.00	-34.3	3.2	A0323
NGC 288	S0193	5.89	0.03	13.19	11.87	-39.7	3.0	A0077
NGC 288	S0414	4.80	0.18	17.02	16.14	-40.5	4.2	A0328
NGC 288	S0198	5.24	0.10	15.62	14.68	-38.4	4.8	
NGC 288	S0028	4.94	0.26	17.39	16.57	-43.9	4.0	
NGC 288	S0027	5.07	0.09	15.40	14.45	-59.5	4.1	A0217
NGC 288	S0113	4.62	0.15	16.38	15.50	-44.5	4.4	
NGC 288	S0020	4.61	0.18	16.72	15.86	-53.0	4.0	
NGC 288	S0017	4.80	0.16	16.51	15.66	-47.5	3.8	A0205
NGC 288	S0012	5.83	0.05	14.46	13.39	-40.9	5.7	A0181
NGC 288	S0006	3.94	0.25	17.22	16.38	-51.7	3.0	

Table 1—Continued

Cluster	Id	ΣCa	$\sigma_{\Sigma\text{Ca}}$	V	I	V–r	σ_{V_r}	Comments
NGC 288	S0004	4.13	0.19	16.85	15.99	-45.1	3.7	
NGC 288	S0124	6.07	0.05	14.08	12.97	-47.5	28.6	A0195
NGC 288	S0161	5.51	0.09	15.11	14.12	-34.1	3.5	A0154
NGC 288	S0107	4.83	0.12	16.18	15.28	-51.3	4.6	
NGC 288	S0065	5.15	0.11	15.84	14.91	-41.9	4.3	A0129
NGC 288	S0061	5.34	0.10	15.43	14.46	-45.0	4.3	A0125
NGC 288	S0059	4.90	0.20	17.10	16.25	-46.6	4.3	A0359
NGC 288	S0058	4.75	0.11	16.06	15.15	-40.4	3.8	A0141
NGC 288	S0054	4.81	0.17	16.82	15.96	-24.7	3.2	No member
NGC 288	S0052	4.29	0.19	17.04	16.22	-42.4	4.2	
NGC 288	S0047	4.44	0.16	16.73	15.87	-27.8	4.0	Member?
NGC 288	S0103	6.48	0.03	13.92	12.74	-42.3	14.9	A0251
NGC 288	S0035	4.67	0.14	16.58	15.72	-37.8	3.6	
NGC 362	H1111	6.24	0.10	14.23	...	213.3	5.2	
NGC 362	H1156	5.33	0.14	14.79	...	205.9	2.6	
NGC 362	H1159	7.38	0.05	12.68	...	209.5	5.4	
NGC 362	H1211	6.10	0.11	14.32	...	206.6	5.7	
NGC 362	H1216	7.28	0.05	13.09	...	217.7	5.7	
NGC 362	H1423	7.63	0.03	12.58	...	217.7	4.1	
NGC 362	H1312	6.80	0.06	13.54	...	196.2	5.3	
NGC 362	H1351	5.81	0.14	14.84	...	207.3	5.9	

Table 1—Continued

Cluster	Id	ΣCa	$\sigma_{\Sigma\text{Ca}}$	V	I	V–r	σ_{V_r}	Comments
NGC 362	H1412	6.45	0.07	13.81	...	218.5	5.1	
NGC 362	H1422	6.50	0.07	13.52	...	218.5	4.8	
NGC 362	H1441	7.68	0.03	12.71	...	217.2	4.1	
NGC 362	H2108	6.52	0.07	13.77	...	211.4	4.8	
NGC 362	H2220	5.46	0.15	15.00	...	215.1	4.8	
NGC 362	H2302	6.26	0.06	13.96	...	207.8	6.7	
NGC 362	H2309	5.85	0.10	14.83	...	215.6	5.2	
NGC 362	H2423	7.50	0.03	12.81	...	228.4	3.2	
NGC 1851	S0160	5.75	0.21	15.51	14.51	290.1	8.4	Member?
NGC 1851	S0275	6.15	0.26	13.92	12.82	324.4	7.6	
NGC 1851	S0109	6.08	0.18	14.85	13.71	321.0	14.4	
NGC 1851	S0195	5.55	0.28	15.82	...	326.1	9.2	
NGC 1851	S0095	7.42	0.09	13.57	12.09	329.0	10.2	
NGC 1851	S0126	6.72	0.09	14.29	13.04	319.5	10.8	
NGC 1851	S0123	5.21	0.32	16.21	15.58	328.0	7.3	
NGC 1851	S0112	7.02	0.09	13.80	12.37	319.8	8.9	
NGC 1851	S0003	7.25	0.07	13.60	12.16	319.8	8.9	
NGC 1851	S0231	5.20	0.33	15.93	14.93	328.9	5.5	
NGC 1851	S0209	6.93	0.11	14.08	12.82	317.9	7.6	
NGC 1851	S0107	6.87	0.17	14.50	...	317.1	8.5	
NGC 1851	S0179	5.45	0.32	16.45	...	324.6	8.9	

Table 1—Continued

Cluster	Id	ΣCa	$\sigma_{\Sigma\text{Ca}}$	V	I	V-r	σ_{V_r}	Comments
NGC 1851	S0175	5.05	0.37	16.22	...	322.8	7.9	
NGC 1851	S0065	5.45	0.27	15.75	14.75	324.9	8.0	
NGC 1904	S0006	4.88	0.21	15.27	...	226.6	8.7	
NGC 1904	S0011	4.74	0.29	15.74	...	228.0	8.0	
NGC 1904	S0015	6.59	0.07	13.22	...	227.7	9.6	
NGC 1904	S0045	4.91	0.26	15.58	...	235.1	8.0	
NGC 1904	S0089	5.07	0.18	14.71	...	225.4	9.2	
NGC 1904	S0091	4.44	0.48	16.25	...	228.2	6.5	
NGC 1904	S0111	4.89	0.28	15.62	...	220.9	8.0	
NGC 1904	S0115	4.47	0.45	15.97	...	224.8	7.4	
NGC 1904	S0138	3.72	0.35	16.16	...	219.8	8.0	
NGC 1904	S0153	6.46	0.07	13.44	...	213.7	9.1	
NGC 1904	S0160	6.15	0.06	13.02	...	219.1	10.3	
NGC 1904	S0161	4.23	0.36	15.86	...	232.0	6.8	
NGC 1904	S0176	4.86	0.19	14.95	...	231.2	8.0	
NGC 1904	S0209	5.28	0.19	15.02	...	233.3	7.6	
NGC 1904	S0224	4.71	0.36	16.09	...	230.1	6.0	
NGC 1904	S0237	5.86	0.17	14.19	...	227.5	8.0	
NGC 1904	S0241	5.93	0.10	13.61	...	230.9	8.3	
Berkeley 20	W0005	7.52	0.04	14.80	13.31	71.2	9.1	
Berkeley 20	W0008	7.37	0.05	15.15	13.72	75.7	8.8	

Table 1—Continued

Cluster	Id	ΣCa	$\sigma_{\Sigma\text{Ca}}$	V	I	V–r	σ_{V_r}	Comments
Berkeley 20	W0012	6.67	0.09	16.21	14.93	82.4	8.8	
Berkeley 20	W0022	6.24	0.13	16.90	15.72	89.6	1.5	
Berkeley 20	W0027	6.34	0.14	17.07	15.87	-6.4	7.4	No member
Berkeley 20	W0029	5.46	0.17	17.14	16.01	39.5	8.1	No member
NGC 2141	W0661	7.76	0.11	14.60	13.26	25.4	7.5	
NGC 2141	W0954	7.70	0.15	14.94	13.55	25.0	7.2	
NGC 2141	W1007	9.03	0.05	13.27	11.42	27.6	8.7	
NGC 2141	W1809	7.87	0.15	14.85	13.50	36.7	7.9	
NGC 2141	W2080	7.73	0.10	14.61	12.91	51.4	8.4	
NGC 2141	W3127	9.45	0.04	13.05	...	35.0	7.7	
NGC 2141	W9999	7.08	0.18	15.00	...	47.6	8.4	
NGC 2141	W0069	8.75	0.15	13.25	11.24	98.6	5.7	No member
NGC 2141	W0330	7.97	0.14	14.01	12.23	17.8	6.0	
NGC 2141	W0847	6.18	0.11	11.82	9.78	15.6	6.8	
NGC 2141	W1401	8.12	0.21	13.25	11.31	24.6	5.9	
NGC 2141	W1602	9.92	0.14	13.66	11.89	28.5	6.0	
NGC 2141	W2111	9.40	0.13	13.30	11.36	41.9	6.5	
NGC 2141	W2703	7.98	0.17	14.05	12.42	35.6	6.2	
NGC 2141	W0514	8.26	0.04	14.09	12.48	34.9	3.1	
NGC 2141	W0587	6.43	0.06	15.14	13.69	70.5	3.1	No member
NGC 2141	W0632	6.74	0.10	15.78	14.38	108.6	2.3	No member

Table 1—Continued

Cluster	Id	ΣCa	$\sigma_{\Sigma\text{Ca}}$	V	I	V–r	σ_{V_r}	Comments
NGC 2141	W0701	7.05	0.10	15.81	14.35	33.5	3.1	
NGC 2141	W0714	7.16	0.08	15.46	13.95	21.5	2.9	
NGC 2141	W0783	7.60	0.06	15.01	13.55	23.9	2.5	
NGC 2141	W0871	6.63	0.06	15.30	13.79	33.0	2.8	
NGC 2141	W1020	7.08	0.08	15.62	14.25	43.0	2.9	
NGC 2141	W1093	7.47	0.06	14.97	13.46	8.0	2.9	No member
NGC 2141	W1194	7.34	0.08	14.90	13.47	12.5	2.7	
NGC 2141	W1205	3.61	0.01	11.58	9.69	39.7	2.3	
NGC 2141	W1267	7.56	0.04	14.53	12.96	21.9	2.7	
NGC 2141	W1333	7.70	0.06	15.09	13.62	22.5	2.9	
NGC 2141	W1348	8.78	0.02	13.25	11.31	0.5	2.2	No member
NGC 2141	W1470	7.73	0.06	15.00	13.56	34.0	2.9	
NGC 2141	W1602	8.66	0.02	13.05	10.88	-7.1	2.3	No member
NGC 2141	W1640	7.49	0.06	15.01	13.53	58.0	2.7	Member?
NGC 2141	W1657	6.72	0.08	15.53	14.19	110.9	3.1	No member
NGC 2141	W1770	7.73	0.05	14.98	13.38	37.1	2.8	
NGC 2141	W1821	8.15	0.04	14.13	12.52	10.5	2.5	No member
NGC 2141	W2066	8.52	0.04	14.18	12.56	49.6	2.7	
NGC 2141	W2082	7.37	0.07	15.45	14.06	39.7	2.3	
NGC 2141	W2167	7.66	0.06	14.91	13.47	30.7	3.1	
Collinder 110	W1148	8.38	0.14	12.97	11.36	37.8	6.2	

Table 1—Continued

Cluster	Id	ΣCa	$\sigma_{\Sigma\text{Ca}}$	V	I	V-r	σ_{V_r}	Comments
Collinder 110	W1218	10.23	0.11	11.47	8.93	56.0	6.7	
Collinder 110	W1306	9.43	0.12	12.62	10.16	78.2	7.0	No member
Collinder 110	W1319	7.59	0.22	12.90	11.28	40.9	5.9	
Collinder 110	W2202	9.17	0.16	11.80	9.76	54.7	7.0	
Collinder 110	W4111	9.16	0.17	12.11	10.17	55.0	7.0	
Collinder 110	W4204	8.28	0.15	12.70	11.11	35.9	6.1	
Collinder 110	W4222	8.30	0.15	12.64	...	56.4	6.8	
Collinder 110	W5002	8.91	0.10	11.89	...	39.1	5.8	
Collinder 110	W5006	7.36	0.16	13.37	...	39.3	5.5	
Collinder 110	W5007	6.87	0.16	13.47	...	36.9	6.1	
Collinder 110	W5008	7.67	0.21	13.31	...	41.2	6.0	
Trumpler 5	W0833	7.07	0.42	14.92	12.94	39.8	6.4	
Trumpler 5	W1026	6.49	0.30	14.71	12.79	29.7	6.3	
Trumpler 5	W1214	7.38	0.31	13.90	11.90	34.4	7.8	
Trumpler 5	W1277	1.54	0.10	14.92	...	331.8	56.3	No member
Trumpler 5	W2280	6.49	0.35	15.18	14.21	35.9	8.3	
Trumpler 5	W2324	6.93	0.30	15.03	13.22	41.6	7.5	
Trumpler 5	W2579	6.43	0.29	16.74	13.78	40.9	7.2	
Trumpler 5	W3066	6.94	0.29	14.39	12.54	37.7	8.4	
Trumpler 5	W3354	7.06	0.27	14.46	12.49	29.2	7.9	
Trumpler 5	W3763	7.80	0.28	14.54	12.72	-20.6	8.3	No member

Table 1—Continued

Cluster	Id	ΣCa	$\sigma_{\Sigma\text{Ca}}$	V	I	V-r	σ_{V_r}	Comments
Trumpler 5	W1063	7.02	0.17	14.46	12.56	51.8	5.8	
Trumpler 5	W1305	8.12	0.21	14.24	12.20	61.0	6.7	
Trumpler 5	W1378	8.35	0.09	13.36	11.38	42.9	6.8	
Trumpler 5	W1935	8.21	0.09	12.87	10.78	45.9	6.9	
Trumpler 5	W4219	8.18	0.12	12.55	10.31	31.4	5.7	TiO
Trumpler 5	W4811	7.61	0.32	13.71	12.00	54.0	7.0	
Trumpler 5	W5099	8.89	0.20	12.35	10.27	48.7	7.0	
Trumpler 5	W6075	8.55	0.19	13.24	10.94	63.2	5.3	
NGC 2298	A0004	4.97	0.06	13.55	12.10	164.4	5.8	
NGC 2298	A0006	4.98	0.06	13.82	12.38	158.1	6.4	
NGC 2298	A0012	4.72	0.07	14.23	12.88	147.2	3.4	
NGC 2298	A0015	4.07	0.10	14.86	13.53	164.3	5.7	
NGC 2298	A0022	3.57	0.13	15.30	14.10	176.2	5.3	
NGC 2298	A0025	3.69	0.16	15.69	14.60	171.7	4.5	
NGC 2298	A0024	4.11	0.16	15.57	14.69	150.3	4.8	
NGC 2298	A9999	3.80	0.18	169.9	6.2	
Berkeley 32	W1851	4.72	0.26	13.49	12.33	40.3	6.5	
Berkeley 32	W1948	5.07	0.18	13.42	12.21	111.4	6.5	
Berkeley 32	W3198	5.78	0.14	12.69	11.51	91.0	1.1	
Berkeley 32	W3199	6.17	0.16	12.78	11.55	80.5	6.0	
Berkeley 32	W3200	5.30	0.18	12.92	11.61	38.1	6.2	No member

Table 1—Continued

Cluster	Id	ΣCa	$\sigma_{\Sigma\text{Ca}}$	V	I	V-r	σ_{V_r}	Comments
Berkeley 32	W3201	6.32	0.17	12.90	11.47	107.5	6.1	
Melotte 66	W783	6.94	0.14	14.58	13.25	15.5	8.3	
Melotte 66	W797	7.39	0.10	14.01	12.65	3.8	7.9	Member?
Melotte 66	W862	7.15	0.11	14.16	12.84	29.3	9.3	
Melotte 66	W968	6.57	0.22	15.48	14.29	16.2	7.9	
Melotte 66	W1000	6.66	0.13	14.68	13.39	10.9	7.8	
Melotte 66	W1209	7.02	0.11	14.17	12.77	15.2	8.0	
Melotte 66	W1419	6.93	0.13	14.48	13.30	17.7	7.8	
Melotte 66	W1615	7.68	0.10	13.66	12.33	43.9	7.6	No member
Melotte 66	W1677	8.33	0.06	13.25	11.53	16.2	8.0	
Melotte 66	W1805	6.96	0.16	14.71	13.52	17.1	7.9	
Melotte 66	W1941	5.19	0.20	15.29	13.95	9.2	7.2	
Melotte 66	W2155	7.04	0.18	14.46	13.29	31.2	7.1	
Melotte 66	W2160	7.38	0.14	14.09	12.74	7.9	6.3	
Melotte 66	W2236	8.18	0.07	12.78	11.00	22.9	0.6	
Berkeley 39	W1587	7.42	0.12	14.43	13.19	58.3	9.1	
Berkeley 39	W1725	7.16	0.13	14.78	13.49	58.3	8.2	
Berkeley 39	W1923	6.71	0.16	15.52	14.19	58.1	8.4	
Berkeley 39	W2033	7.42	0.11	14.33	...	56.4	8.7	
Berkeley 39	W2055	7.60	0.08	13.99	12.49	58.1	8.2	
Berkeley 39	W2573	7.19	0.12	14.74	13.50	58.5	9.3	

Table 1—Continued

Cluster	Id	ΣCa	$\sigma_{\Sigma\text{Ca}}$	V	I	$V-r$	σ_{V_r}	Comments
Berkeley 39	W2784	7.33	0.10	14.20	13.00	53.9	8.6	
Berkeley 39	W4368	8.23	0.07	13.55	...	61.4	8.2	
Berkeley 39	W9999	5.97	0.17	73.5	7.2	
NGC 2420	W0034	4.05	0.20	13.09	12.08	73.1	6.3	
NGC 2420	W0041	5.70	0.17	12.67	11.59	69.1	6.3	
NGC 2420	W0073	8.34	0.13	11.09	9.66	77.9	5.9	
NGC 2420	W0114	5.16	0.19	13.10	12.10	67.6	6.3	
NGC 2420	W0140	6.95	0.16	11.53	10.26	63.1	1.7	
NGC 2420	W0188	5.62	0.32	13.48	12.54	71.8	6.0	
NGC 2420	W0192	5.54	0.20	12.94	11.91	67.5	6.5	
NGC 2506	W2101	8.04	0.17	11.09	9.66	79.8	7.5	
NGC 2506	W2122	6.58	0.20	13.10	12.10	78.9	7.1	
NGC 2506	W2212	4.78	0.20	11.53	10.26	28.9	7.0	No member
NGC 2506	W3254	6.73	0.13	12.94	11.91	76.2	6.3	
NGC 2682	W0141	7.85	0.04	10.48	9.40	35.1	3.761	
NGC 2682	W0105	7.55	0.03	10.30	9.07	41.0	2.507	
NGC 2682	W0185	6.50	0.08	11.06	10.80	42.9	1.247	
NGC 2682	W0174	6.62	0.13	12.72	12.02	34.6	2.975	
NGC 2682	W0143	5.67	0.06	11.52	10.61	38.2	3.033	
NGC 2682	W0103	5.81	0.18	13.17	12.52	32.3	3.108	
NGC 2682	W0164	7.43	0.03	10.55	9.46	37.5	2.732	

Table 1—Continued

Cluster	Id	ΣCa	$\sigma_{\Sigma\text{Ca}}$	V	I	V–r	σ_{V_r}	Comments
NGC 2682	W0104	7.17	0.05	11.20	10.12	31.7	2.903	
NGC 2682	W0096	6.52	0.14	13.02	12.10	31.1	3.132	
NGC 2682	W0100	6.38	0.19	13.49	12.78	37.7	2.372	
NGC 2682	W0132	5.90	0.15	13.10	12.38	38.5	2.687	
NGC 2682	W0108	8.51	0.02	9.72	8.36	35.0	0.694	
NGC 2682	W0116	5.47	0.23	14.16	13.35	33.7	2.201	
NGC 2682	W0111	6.00	0.13	12.73	12.04	41.7	3.046	
NGC 2682	W0135	7.55	0.05	11.44	10.39	39.5	2.747	
NGC 2682	W0130	6.30	0.14	12.89	12.30	43.4	3.098	
NGC 2682	W0127	6.55	0.13	12.76	12.08	38.2	2.176	
NGC 2682	W0117	5.41	0.10	12.60	11.69	37.1	2.223	
NGC 2682	W0170	8.09	0.02	9.69	8.36	17.9	2.548	Member?
NGC 2682	W0173	6.38	0.31	12.11	11.08	21.0	6.466	Member?
NGC 2682	W2152	6.31	0.22	10.93	9.79	36.4	6.591	
NGC 2682	W6495	8.30	0.11	9.37	7.87	34.5	6.185	
NGC 3201	S0011	4.89	0.19	14.55	13.30	488.9	0.3	
NGC 3201	S0082	5.16	0.17	14.60	13.31	489.5	0.2	
NGC 3201	S0165	6.30	0.17	12.71	11.20	496.0	0.4	
NGC 3201	S0253	8.89	0.74	16.74	15.63	35.6	0.8	No member
NGC 3201	S0272	7.30	0.24	14.90	13.64	34.8	0.8	No member
NGC 3201	S0278	5.77	0.18	12.91	11.51	495.1	0.3	

Table 1—Continued

Cluster	Id	ΣCa	$\sigma_{\Sigma\text{Ca}}$	V	I	$V-r$	σ_{V_r}	Comments
NGC 3201	S0287	8.27	0.10	13.27	11.89	27.1	0.7	No member
NGC 3201	S0288	5.63	0.10	13.43	12.11	490.3	0.3	
NGC 3201	S0296	6.42	0.05	12.64	11.08	488.1	0.4	
NGC 3201	S0298	4.12	0.18	15.52	14.28	492.4	0.4	
NGC 3201	S0302	4.34	0.20	14.87	13.64	490.1	0.3	
NGC 3201	S0320	4.46	0.15	15.21	14.03	493.3	0.2	
NGC 3201	S0323	6.93	0.05	12.39	10.68	490.7	0.4	
NGC 4590	S164	6.48	0.34	15.16	16.02	-36.7	0.1	No member
NGC 4590	S174	6.17	0.61	15.95	16.64	-6.2	0.6	No member
NGC 4590	S189	6.02	0.41	15.14	15.79	-21.3	0.7	No member
NGC 4590	S190	7.26	0.39	15.31	16.05	-47.4	0.8	No member
NGC 4590	S194	5.74	0.39	15.25	16.11	-22.2	0.6	No member
NGC 4590	S195	3.55	0.16	14.20	15.11	-95.3	0.7	
NGC 4590	S203	4.03	0.14	13.36	14.44	-95.3	0.1	
NGC 4590	S206	3.50	0.26	14.58	15.43	-97.7	1.0	
NGC 4590	S207	5.18	0.08	12.67	14.00	-99.4	0.8	
NGC 4590	S208	5.58	0.53	15.98	16.71	81.1	0.7	No member
NGC 4590	S221	6.38	0.17	13.68	14.58	-24.4	0.9	No member
NGC 4590	S227	3.31	0.24	14.52	15.38	-94.2	1.1	
NGC 4590	S230	5.82	0.95	16.76	17.52	27.0	0.5	No member
NGC 4590	S237	3.01	0.32	15.01	15.83	-90.5	0.8	

Table 1—Continued

Cluster	Id	ΣCa	$\sigma_{\Sigma\text{Ca}}$	V	I	V-r	σ_{V_r}	Comments
NGC 4590	S250	7.16	0.24	14.52	15.46	192.6	0.6	No member
NGC 4590	S255	3.34	0.25	14.69	15.54	-95.6	0.9	
NGC 4590	S259	6.23	0.45	14.69	15.54	-30.5	0.8	No member
NGC 4590	S265	3.23	0.35	14.93	15.74	-93.1	0.8	
NGC 4590	S266	4.23	0.49	14.93	15.74	-22.6	0.9	No member
NGC 4590	S270	5.91	1.09	16.32	17.05	-0.2	1.0	No member
NGC 4590	S277	3.06	0.58	17.79	18.76	-4.7	0.5	No member
NGC 4590	S286	2.92	0.43	15.59	16.36	-91.5	0.7	
NGC 4590	S113	6.85	0.22	15.45	...	-21.7	3.2	No member
NGC 4590	S134	8.06	0.36	15.53	...	-8.5	2.7	No member
NGC 4590	H2	2.77	0.21	14.95	...	-84.6	23.7	
NGC 4590	H47	2.87	0.16	15.15	...	-87.4	24.2	
NGC 4590	H49	2.97	0.20	14.62	...	-82.0	22.6	
NGC 4590	H74	3.25	0.17	14.66	...	-89.8	26.2	
NGC 4590	H119	3.74	0.07	13.66	...	-82.3	26.8	
NGC 4590	H239	3.42	0.11	14.19	...	-84.1	24.3	
NGC 4590	H256	4.44	0.05	12.64	...	-76.9	26.8	
NGC 4590	H258	3.23	0.10	14.36	...	-75.8	27.3	
NGC 4590	H260	4.61	0.04	12.52	...	-95.6	13.8	
NGC 4590	R4	2.20	0.26	14.71	13.68	-88.6	6.4	
NGC 4590	R5	3.97	0.24	13.41	12.23	-40.0	6.4	No member

Table 1—Continued

Cluster	Id	ΣCa	$\sigma_{\Sigma\text{Ca}}$	V	I	$V-r$	σ_{V_r}	Comments
NGC 4590	R9	5.32	0.27	14.49	13.44	202.8	6.7	No member
NGC 4590	R10	5.40	0.11	12.39	10.36	-94.2	5.6	
NGC 4590	R12	3.15	0.15	13.52	12.31	-75.9	7.1	
NGC 4590	R15	3.69	0.28	13.19	11.94	-63.0	7.0	
NGC 4590	R23	5.05	0.22	12.86	11.51	-51.4	7.0	Member?
NGC 5927	Z0141	6.80	0.10	16.99	15.36	-73.8	2.5	
NGC 5927	Z0372	7.96	0.03	15.64	13.42	-78.9	2.8	
NGC 5927	Z0674	8.43	0.02	14.90	12.67	-83.4	3.2	
NGC 5927	Z0692	7.26	0.11	17.28	15.54	-12.8	1.7	No member
NGC 5927	Z1098	8.67	0.03	15.45	13.27	-80.9	2.6	
NGC 5927	Z1355	7.90	0.03	15.77	13.53	-84.0	3.0	
NGC 5927	Z1694	8.23	0.03	15.84	13.59	-78.4	2.7	
NGC 5927	Z2548	8.30	0.02	14.94	12.61	-70.6	2.4	
NGC 5927	Z2776	7.53	0.04	16.11	14.25	-80.4	3.1	
NGC 5927	Z3179	7.07	0.06	16.42	14.76	-73.6	3.4	
NGC 5927	Z3196	7.56	0.04	15.72	13.99	-76.4	2.8	
NGC 5927	Z4098	8.23	0.02	15.11	12.65	-88.6	2.7	
NGC 5927	Z4379	8.46	0.03	14.94	12.72	-78.8	2.7	
NGC 5927	Z4641	7.93	0.04	15.73	13.77	-58.9	2.6	Member?
NGC 5927	Z4873	7.71	0.04	15.64	13.85	-77.1	2.6	
NGC 5927	Z4976	8.21	0.03	15.52	13.36	-74.0	2.5	

Table 1—Continued

Cluster	Id	ΣCa	$\sigma_{\Sigma\text{Ca}}$	V	I	V-r	σ_{V_r}	Comments
NGC 5927	Z5433	8.67	0.03	15.09	12.79	-57.5	2.2	Member?
NGC 5927	Z5642	7.85	0.03	15.48	13.34	-82.2	2.7	
NGC 5927	Z6925	8.39	0.02	14.92	12.58	-97.6	3.0	
NGC 5927	Z204901	8.34	0.03	15.45	13.42	-77.7	2.4	
NGC 5927	Z206658	8.50	0.02	14.82	12.41	-88.8	2.9	
NGC 5927	Z210840	9.76	0.02	14.89	12.74	-91.1	2.4	
NGC 5927	Z211700	8.24	0.02	14.93	12.53	-92.0	2.8	
NGC 5927	Z212159	8.34	0.02	15.03	12.81	-78.3	2.4	
NGC 5927	Z212828	7.74	0.03	14.58	12.46	-28.6	3.0	No member
NGC 5927	Z213516	7.90	0.08	17.26	15.54	30.5	2.3	No member
NGC 6352	Z0541	6.90	0.04	14.65	13.23	-113.6	3.9	
NGC 6352	Z0934	6.68	0.05	15.23	13.88	-105.8	3.4	
NGC 6352	Z1346	6.65	0.04	15.20	13.83	-116.0	3.2	
NGC 6352	Z1924	7.65	0.08	14.87	13.44	-87.9	2.3	Member?
NGC 6352	Z2393	6.18	0.08	16.00	14.69	-113.4	3.4	
NGC 6352	Z3467	6.62	0.04	15.03	13.68	-113.5	3.6	
NGC 6352	Z3925	6.13	0.07	16.05	14.79	-119.5	3.3	
NGC 6352	Z4396	6.84	0.05	15.31	13.92	-114.3	3.5	
NGC 6352	Z4688	7.50	0.02	14.17	12.57	-110.6	3.1	
NGC 6352	Z5131	7.53	0.07	15.34	14.00	-91.5	2.5	Member?
NGC 6352	Z5424	5.84	0.07	15.21	13.89	-111.8	3.2	

Table 1—Continued

Cluster	Id	ΣCa	$\sigma_{\Sigma\text{Ca}}$	V	I	V-r	σ_{V_r}	Comments
NGC 6352	Z5673	7.30	0.02	13.58	11.66	-116.6	3.1	
NGC 6352	Z6343	6.90	0.05	14.81	13.32	-103.7	3.5	
NGC 6352	Z6611	6.77	0.05	15.19	13.79	-114.0	3.6	
NGC 6352	Z6811	7.75	0.04	14.37	13.03	-2.2	3.5	No member
NGC 6352	Z202750	4.75	0.03	14.96	13.63	-11.6	2.6	No member
NGC 6352	Z7496	6.82	0.07	15.96	14.59	-80.1	3.2	
NGC 6352	Z7708	7.26	0.04	14.99	13.63	-14.2	3.9	No member
NGC 6352	z7876	7.29	0.04	14.71	13.36	-168.3	3.6	No member
NGC 6352	Z8025	6.49	0.05	15.35	13.99	-90.7	3.6	
NGC 6352	Z0141	6.99	0.14	17.08	15.79	-7.9	4.9	No member
NGC 6352	Z0458	6.56	0.04	15.08	13.72	-117.9	3.8	
NGC 6352	Z0657	7.16	0.08	16.10	14.84	-72.9	4.3	
NGC 6352	Z0831	7.52	0.03	14.44	12.90	-116.9	1.6	
NGC 6352	Z1139	6.55	0.08	15.93	14.61	-43.9	3.8	No member
NGC 6352	Z1503	6.08	0.08	15.87	14.58	-113.0	4.2	
NGC 6352	Z1728	7.83	0.02	13.68	11.99	-128.6	2.7	
NGC 6352	Z2023	7.58	0.02	13.38	11.63	-120.6	2.4	
NGC 6352	Z2336	7.62	0.08	15.65	14.20	-166.9	2.8	
NGC 6352	Z2586	7.08	0.03	14.41	12.94	-117.9	3.0	
NGC 6352	Z2950	7.53	0.07	16.00	14.57	-86.8	4.1	Member?
NGC 6352	Z3302	6.81	0.04	15.08	13.69	-110.8	3.6	

Table 1—Continued

Cluster	Id	ΣCa	$\sigma_{\Sigma\text{Ca}}$	V	I	V-r	σ_{V_r}	Comments
NGC 6352	Z201006	7.27	0.04	15.14	13.79	-114.7	3.3	
NGC 6352	Z4171	6.09	0.10	16.58	15.36	-118.4	5.0	
NGC 6352	Z4626	6.82	0.05	15.17	13.82	-123.7	6.4	
NGC 6352	Z5000	6.78	0.04	15.00	13.63	-122.2	2.7	
NGC 6528	O0256	7.81	0.11	16.18	2.02	219.4	4.1	
NGC 6528	O0409	8.06	0.07	16.41	1.96	209.6	4.0	
NGC 6528	O0572	7.19	0.05	15.90	1.90	-75.7	3.7	No member
NGC 6528	O0682	8.98	0.09	15.81	2.07	212.3	4.3	
NGC 6528	O0809	8.56	0.12	16.69	3.04	-32.1	4.0	No member
NGC 6528	O0927	7.22	0.20	16.68	1.86	226.6	4.2	
NGC 6528	O0986	8.38	0.10	16.08	2.14	236.1	5.0	
NGC 6681	H0030	4.85	0.28	15.73	...	165.3	3.4	
NGC 6681	H0069	6.69	0.20	15.49	...	204.6	2.3	
NGC 6681	H0102	5.05	0.13	15.04	13.96	202.5	6.1	
NGC 6681	H0119	6.20	0.13	13.79	...	174.7	5.1	No member
NGC 6681	H0122	5.11	0.04	14.89	...	179.6	5.3	
NGC 6681	H0166	6.92	0.13	15.56	...	-94.9	3.1	No member
NGC 6681	H0260	4.59	0.08	15.36	...	188.9	4.8	
NGC 6681	R0031	6.92	0.07	15.06	14.01	93.5	6.1	No member
NGC 6681	R0202	5.56	0.16	13.98	12.80	181.2	6.0	
NGC 6681	R0387	5.43	0.09	14.50	13.36	171.3	6.1	

Table 1—Continued

Cluster	Id	ΣCa	$\sigma_{\Sigma\text{Ca}}$	V	I	$V-r$	σ_{V_r}	Comments
NGC 6705	S2441	7.54	0.21	13.40	12.05	27.8	1.1	
NGC 6705	S2680	7.50	0.74	12.91	11.55	22.4	0.6	
NGC 6705	S4002	9.37	0.19	11.43	9.86	35.6	0.1	
NGC 6705	S4390	8.81	0.17	12.86	11.16	18.2	0.9	
NGC 6705	S4509	7.51	1.30	12.83	11.51	-4.3	0.6	No member
NGC 6705	S4780	8.36	0.39	12.00	10.52	36.2	0.1	
NGC 6705	S4961	8.69	0.33	12.56	10.73	-30.8	0.9	No member
NGC 6705	S5107	6.55	1.14	13.38	11.89	7.2	1.2	Member??
NGC 6705	S5527	8.71	0.23	11.62	10.12	33.3	0.0	
NGC 6705	S5656	6.99	0.58	13.10	11.61	384.6	0.6	No member
NGC 6705	S5688	9.12	0.53	11.65	9.90	25.6	1.0	
NGC 6705	S5866	8.92	0.47	12.45	10.55	16.3	0.8	
NGC 6705	S6410	7.59	0.91	11.86	10.35	68.7	1.0	
NGC 6705	S6493	9.24	0.73	11.41	9.79	30.5	0.7	
NGC 6705	S6675	7.64	1.46	11.83	10.48	66.6	1.2	
NGC 6705	S7099	8.57	1.09	11.46	10.08	40.7	0.7	
NGC 6705	S7240	8.86	2.00	11.43	9.74	40.4	0.6	
NGC 6705	S7442	7.76	2.57	11.90	10.43	53.8	0.5	
NGC 6705	S8287	8.84	0.09	11.63	10.10	33.4	1.0	
NGC 6705	S8354	7.87	0.59	13.22	11.63	107.3	0.7	No member
NGC 6705	S9264	8.21	1.02	13.27	11.51	8.6	0.7	No member

Table 1—Continued

Cluster	Id	ΣCa	$\sigma_{\Sigma\text{Ca}}$	V	I	$V-r$	σ_{V_r}	Comments
NGC 6705	S9751	7.541	0.54	11.56	9.88	81.2	0.9	No member
NGC 6715	R66	6.51	0.08	15.34	13.93	155.9	5.2	
NGC 6715	R137	6.35	0.10	15.71	14.21	161.2	5.8	
NGC 6715	R200	6.70	0.12	15.92	14.52	152.3	4.6	
NGC 6715	R202	4.98	0.14	15.92	14.51	159.1	3.6	
NGC 6715	R205	6.19	0.14	15.92	14.47	170.3	4.4	
NGC 6715	R228	6.09	0.12	16.00	14.61	164.1	6.1	
NGC 6715	R328	7.80	0.23	16.32	14.99	-20.0	4.0	No member
NGC 6715	R402	7.44	0.23	16.49	15.16	154.2	3.5	
NGC 6715	R410	6.12	0.29	16.51	15.21	160.2	3.9	
NGC 6715	R438	5.21	0.17	16.58	15.29	144.5	4.3	
NGC 6715	R456	4.82	0.21	16.63	15.42	162.9	3.3	
NGC 6715	R466	5.10	0.17	16.64	15.38	156.8	4.5	
NGC 6715	R558	3.48	0.23	16.84	15.63	208.1	3.5	No member
NGC 6715	R591	5.53	0.28	16.90	15.65	152.0	4.1	
NGC 6715	R617	5.78	0.25	16.95	15.69	155.4	4.4	
NGC 6715	R618	5.79	0.26	16.95	15.70	160.4	4.0	
NGC 6715	R657	6.70	0.26	17.02	15.86	156.	3.4	
NGC 6715	R660	4.66	0.28	17.02	15.90	174.8	3.3	
NGC 6715	R695	6.25	0.27	17.07	15.87	153.3	3.5	
NGC 6715	R822	4.86	0.26	17.27	16.04	186.4	4.1	Member?

Table 1—Continued

Cluster	Id	ΣCa	$\sigma_{\Sigma\text{Ca}}$	V	I	V–r	σ_{V_r}	Comments
NGC 6715	R824	5.85	0.40	17.27	16.10	137.3	2.4	
NGC 6715	R844	3.80	0.29	17.30	16.08	140.7	2.7	
NGC 6715	R882	4.72	0.27	17.33	16.23	156.3	0.8	
NGC 6715	R972	5.06	0.30	17.43	16.26	171.6	2.8	
NGC 6715	R1026	5.59	0.25	17.51	16.34	159.8	3.1	
NGC 6715	R1044	4.36	0.30	17.54	16.41	163.6	3.8	
NGC 6715	R1067	5.73	0.41	17.57	16.41	180.1	3.3	Member?
NGC 6715	R1122	6.98	0.46	17.66	16.82	2.4	2.2	No member
NGC 6715	R1203	4.21	0.39	17.75	16.91	49.5	1.9	No member
NGC 6715	R9991	4.92	0.16	158.6	5.0	
NGC 6715	R9992	6.71	0.29	-38.0	3.0	No member
NGC 6715	R9994	4.51	0.29	-63.5	4.2	No member
NGC 6715	R9995	4.34	0.34	39.2	2.4	No member
NGC 6715	R8881	3.93	0.36	136.8	0.8	
NGC 6715	R8882	6.64	0.40	20.3	3.0	
NGC 6715	R8883	6.04	0.19	160.6	5.4	
NGC 6791	S11539	8.37	0.27	14.21	12.58	-88.7	2.4	No member
NGC 6791	S11814	9.45	0.30	13.85	12.19	-40.0	4.2	
NGC 6791	S1249	8.97	0.26	14.93	13.49	-35.4	2.7	
NGC 6791	S14379	5.65	0.20	13.84	10.78	-18.8	1.7	Member?
NGC 6791	S99999	8.20	0.41	7.1	2.0	No member

Table 1—Continued

Cluster	Id	ΣCa	$\sigma_{\Sigma\text{Ca}}$	V	I	V–r	σ_{V_r}	Comments
NGC 6791	S14591	8.88	0.35	13.84	10.78	-41.1	2.6	
NGC 6791	S2044	7.62	0.38	14.14	12.67	-41.1	2.3	
NGC 6791	S3754	8.20	0.44	14.61	13.08	-42.8	2.8	
NGC 6791	S4952	8.74	0.35	14.71	13.23	-35.6	2.6	
NGC 6791	S5342	9.15	0.26	14.14	12.39	-49.9	3.3	
NGC 6791	S5839	9.42	0.22	13.75	11.77	-34.5	3.3	
NGC 6791	S8266	9.22	0.18	13.74	11.96	-63.4	2.3	
NGC 6791	S8904	8.83	0.27	13.86	11.89	-59.6	2.6	
NGC 6791	S2793	9.83	0.40	14.10	12.08	-41.0	0.3	
NGC 6791	S4616	9.70	0.36	16.13	14.86	-36.8	3.4	
NGC 6791	S5454	8.91	0.64	14.92	13.51	-57.9	3.0	
NGC 6791	S5972	7.22	0.82	15.86	14.57	-58.9	2.0	
NGC 6791	S6583	9.60	0.63	16.34	15.10	-73.9	2.0	
NGC 6791	S7912	8.97	0.65	15.70	14.38	-87.8	2.4	No member
NGC 6791	S7972	9.19	0.29	14.14	12.37	-48.0	0.4	
NGC 6819	W390	7.67	0.16	12.76	11.56	-4.8	5.0	
NGC 6819	W965	8.97	0.09	11.85	10.29	-0.9	5.9	
NGC 6819	W968	9.32	0.11	11.75	10.08	-7.7	6.1	
NGC 6819	W970	8.65	0.06	11.57	9.36	-38.6	3.7	No member
NGC 6819	W972	8.55	0.09	12.03	10.52	-2.0	5.8	
NGC 6819	W974	7.94	0.12	12.67	11.40	3.7	5.0	

Table 1—Continued

Cluster	Id	ΣCa	$\sigma_{\Sigma\text{Ca}}$	V	I	V–r	σ_{V_r}	Comments
NGC 6819	W975	8.36	0.10	12.24	10.90	-4.5	5.2	
NGC 6819	W977	7.93	0.12	12.65	11.36	-3.4	5.1	
NGC 7078	B39	4.39	0.04	12.82	...	-133.2	6.7	Member?
NGC 7078	B44	2.88	0.10	14.63	...	-123.7	5.8	
NGC 7078	B67	3.96	0.06	13.43	...	-118.9	5.6	
NGC 7078	B90	3.58	0.07	13.81	...	-102.0	4.8	
NGC 7078	B137	2.96	0.12	14.89	...	-109.7	4.8	
NGC 7078	B187	3.44	0.10	14.25	...	-92.8	6.0	
NGC 7078	B212	4.17	0.06	13.49	...	-117.0	5.9	
NGC 7078	B248	4.16	0.05	13.09	...	-114.9	4.9	
NGC 7078	B292	3.35	0.08	14.00	...	-115.1	5.5	
NGC 7078	B355	2.71	0.15	14.94	...	-119.3	1.4	
NGC 7078	B414	3.39	0.09	14.13	...	-105.7	5.5	
NGC 7078	B429	3.24	0.09	13.89	12.64	-99.6	5.7	
NGC 7078	B457	2.86	0.09	14.35	...	-92.1	5.6	
NGC 7078	B505	3.81	0.07	13.56	...	-91.1	5.1	
NGC 7078	B575	5.97	0.08	14.03	...	-71.2	5.1	Member?
NGC 7078	B599	3.51	0.06	13.48	...	-73.7	6.0	Member?
NGC 7078	S450	3.51	0.03	13.77	12.62	-104.6	5.9	
NGC 7078	S779	2.84	0.02	12.76	...	-110.2	3.8	
NGC 7078	S454	2.28	0.10	15.71	14.78	-116.3	3.2	

Table 1—Continued

Cluster	Id	ΣCa	$\sigma_{\Sigma\text{Ca}}$	V	I	V–r	σ_{V_r}	Comments
NGC 7078	S478	2.27	0.13	16.42	...	-114.1	2.9	
NGC 7078	S468	6.19	0.10	15.79	...	28.8	2.3	No member
NGC 7078	S801	3.46	0.06	14.51	...	-132.0	53.9	
NGC 7078	S833	4.44	0.03	13.40	...	-115.9	4.0	
NGC 7078	S796	3.43	0.04	14.44	...	-101.0	3.3	
NGC 7078	S831	3.35	0.06	14.42	...	-112.8	3.6	
NGC 7078	S767	2.50	0.17	16.76	...	-106.9	2.0	
NGC 7078	S1343	3.39	0.04	14.36	13.24	-99.4	3.5	
NGC 7078	S769	5.98	0.11	15.77	...	-37.7	3.1	No member
NGC 7078	S784	3.80	0.05	14.11	...	-110.8	3.9	
NGC 7078	S1346	3.88	0.04	13.92	12.77	-111.3	5.9	
NGC 7078	S154	3.58	0.04	14.16	13.07	-102.6	3.5	
NGC 7078	S1354	3.40	0.04	14.17	13.09	-101.3	5.3	
NGC 7078	S173	2.73	0.10	15.84	14.83	-120.9	4.1	
NGC 7078	S177	3.41	0.04	14.12	13.05	-109.0	4.1	
NGC 7078	S168	2.45	0.12	16.42	15.48	-111.2	3.1	
NGC 7078	S448	2.43	0.17	16.76	15.83	-102.4	2.6	
NGC 7078	S455	3.13	0.06	14.84	...	-107.9	2.2	
NGC 7078	S1332	3.85	0.04	13.98	12.82	-119.3	3.7	
NGC 7078	S1337	3.54	0.03	13.81	12.60	-95.2	40.9	
NGC 7078	S677	3.22	0.05	14.46	13.30	-95.2	5.9	

Table 1—Continued

Cluster	Id	ΣCa	$\sigma_{\Sigma\text{Ca}}$	V	I	V–r	σ_{V_r}	Comments
NGC 7078	S694	3.19	0.06	14.88	13.77	-101.0	4.3	
NGC 7078	S708	2.93	0.12	16.49	15.50	-101.8	3.6	
NGC 7078	S109	2.10	0.08	20.35	...	-95.9	2.1	
NGC 7078	S1098	2.61	0.11	16.31	...	-108.2	1.8	
NGC 7078	S499	2.70	0.11	16.16	15.18	-109.2	3.2	
NGC 7078	S434	4.05	0.03	13.68	...	-112.6	158.6	
NGC 7078	S503	3.44	0.05	14.34	13.32	-95.7	5.5	
NGC 7078	S1333	5.26	0.06	14.68	13.56	-114.3	4.9	
NGC 7789	W8957	8.96	0.14	11.61	10.05	-74.3	6.0	
NGC 7789	W9840	9.15	0.13	11.93	10.34	-51.7	6.4	
NGC 7789	W10652	8.33	0.10	11.89	10.21	-56.4	5.2	
NGC 7789	W10746	9.36	0.07	11.04	8.64	-56.9	6.4	
NGC 7789	W1135	8.03	0.14	12.19	10.66	-60.1	5.4	
NGC 7789	W12478	8.77	0.12	11.57	9.88	-56.6	5.7	
NGC 7789	W1269	8.27	0.12	11.96	10.34	-54.1	5.1	
NGC 7789	W13089	8.27	0.15	11.98	10.27	-58.8	5.0	
NGC 7789	W13862	9.46	0.07	10.74	8.53	-60.4	7.4	
NGC 7789	W2740	9.20	0.09	11.05	9.08	-57.5	6.6	
NGC 7789	W6345	9.63	0.07	10.66	8.48	-56.1	6.6	
NGC 7789	W6767	8.94	0.08	11.35	9.57	-58.3	6.3	
NGC 7789	W6810	9.17	0.09	11.61	9.72	-47.6	5.7	

References:

- **NGC 104** Lee (1977) [L], Stetson (2000) [S]
- **NGC 188** Webda <http://obswww.unige.ch/webda/> [W]
- **NGC 288** Alcaïno & Liller (1980) [A]
- **NGC 362** Harris (1982) [H]
- **NGC 1851** Stetson (1981) [S]
- **NGC 1904** Stetson & Harris (1977) [S]
- **Berkeley 20** Webda [W]
- **NGC 2141** Burkhead y col. (1972) [B]; Rosvick (1995) [R]; Webda [W];
- **Collinder 110** Webda [W]
- **Trumpler 5** Webda [W]
- **NGC 2298** Alcaïno & Liller (1986) [A]; Alcaïno (1974) [A]
- **Berkeley 32** Webda [W]
- **Melotte 66** Webda [W]
- **Berkeley 39** Webda [W]
- **NGC 2420** Webda [W]
- **NGC 2506** Webda [W]
- **NGC 2682** Webda [W]
- **NGC 3201** Stetson (2000) [S];

- **NGC 4590** Harris (1975a) [H]; Stetson (2000) [S]
- **NGC 5927** Zoccalli (comunicación privada)
- **NGC 6352** Zoccalli (comunicación privada); Rosenberg y cols. (2000) [R]
- **NGC 6528** Ortolani y cols. (1992) [O]
- **NGC 6681** Harris (1975b) [H]; Rosenberg y cols. (2000) [R]
- **NGC 6705** Sung y cols. (1999) [S]
- **NGC 6715** Rosenberg y cols. (2004) [R]
- **NGC 6791** Stetson y cols (2003) [S]
- **NGC 6819** Webda [W]
- **NGC 7078** Buonanno y cols. (1983) [B]; Stetson (2000) [S]
- **NGC 7789** Webda [W]

Table 1—Continued

Cluster	Id	ΣCa	$\sigma_{\Sigma\text{Ca}}$	V	I	V–r	σ_{V_r}	Comments
NGC 7789	W7013	8.78	0.09	11.32	9.66	-67.9	5.4	
NGC 7789	W7029	9.41	0.07	10.74	8.59	-54.6	7.0	
NGC 7789	W7091	9.22	0.09	11.20	9.36	-48.2	6.7	
NGC 7789	W8293	8.75	0.10	11.46	9.74	-54.9	5.0	
NGC 7789	W8400	9.58	0.08	11.18	9.07	-67.4	6.6	
NGC 7789	W8799	9.46	0.06	10.88	8.77	-56.0	1.1	
NGC 7789	W896	8.64	0.09	11.49	9.74	-60.9	6.2	